



HAL
open science

The enhanced adsorption properties of molecular imprinted polymer material prepared using nitroxide-mediated Radical Deactivation Reversible Polymerization

Soumaya Kouki, Najeh Jaoued-Grayaa, Amira Anene, Emmanuel Beyou, Yves Chevalier, Souhaira Hbaieb

► To cite this version:

Soumaya Kouki, Najeh Jaoued-Grayaa, Amira Anene, Emmanuel Beyou, Yves Chevalier, et al.. The enhanced adsorption properties of molecular imprinted polymer material prepared using nitroxide-mediated Radical Deactivation Reversible Polymerization. *Polymer*, 2022, 249, pp.124841. 10.1016/j.polymer.2022.124841 . hal-03654008

HAL Id: hal-03654008

<https://hal.science/hal-03654008v1>

Submitted on 28 Apr 2022

HAL is a multi-disciplinary open access archive for the deposit and dissemination of scientific research documents, whether they are published or not. The documents may come from teaching and research institutions in France or abroad, or from public or private research centers.

L'archive ouverte pluridisciplinaire **HAL**, est destinée au dépôt et à la diffusion de documents scientifiques de niveau recherche, publiés ou non, émanant des établissements d'enseignement et de recherche français ou étrangers, des laboratoires publics ou privés.

The enhanced adsorption properties of molecular imprinted polymer material prepared using nitroxide-mediated Radical Deactivation Reversible Polymerization

Soumaya Kouki^{a,b,c,d}, Najeh Jaoued-Grayaa^d, Amira Anene^d, Emmanuel Beyou^c, Yves Chevalier^{b*}, Souhaira Hbaieb^{a*}

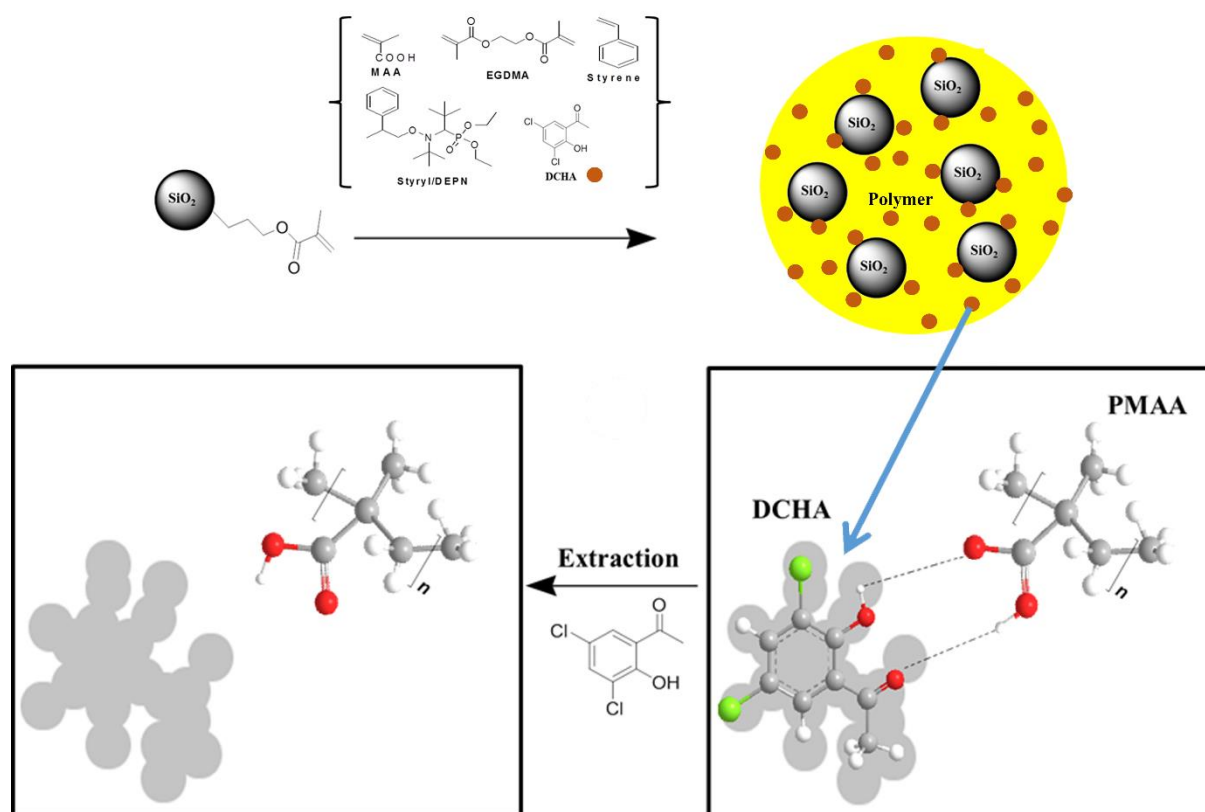
a) Laboratoire de Recherche: Caractérisations, Applications et Modélisation de Matériaux, Université de Tunis El Manar, Faculté des Sciences de Tunis, Campus universitaire El Manar, Tunisia.

b) Laboratoire d'Automatique, de Génie des Procédés et de Génie Pharmaceutique, Université de Lyon 1, UMR 5007 CNRS, 69622 Villeurbanne Cedex, France.

c) Laboratoire Ingénierie des Matériaux Polymères, Université de Lyon 1, UMR 5223, 69622 Villeurbanne, France.

d) Unité Spécialisée de développement des techniques analytiques, Institut National de Recherche et d'Analyse Physico-chimique, Biotechpole Sidi-Thabet, 2020 Ariana, Tunisia.

GRAPHICAL ABSBTRACT



ABSTRACT

The origin of the improved performance of Molecular Imprinted Polymers (MIPs) prepared by Nitroxide-Mediated Radical Deactivation Reversible Polymerization (NMRP) and by conventional Free Radical Polymerization (FRP) was investigated through a detailed interpretation of adsorption onto imprinted- and non-imprinted materials. MIPs designed for the adsorption of 3,5-dichloro-4-hydroxyacetophenone (DCHA) were copolymers of methacrylic acid and styrene cross-linked by ethylene glycol dimethacrylate. Modelling the adsorption

isotherms using the Langmuir–Volmer model showed that the enhanced adsorption to NMRP MIP was due to a higher density of molecular imprints rather than a higher affinity of the molecular imprints for DCHA. Adsorption was exothermic onto molecular imprints and athermal off them; adsorption caused an increase of entropy. The interactions between monomer and DCHA measured in solution and the influence of pH on adsorption pointed out hydrogen bonding between the MIP carboxylic acids and the DCHA phenol group as the main contribution to adsorption.

Keywords: Nitroxide-mediated radical polymerization; Molecularly imprinted materials; Adsorption isotherms.

INTRODUCTION

Molecular imprinted polymer materials (MIPs) are usually prepared by means of radical polymerization of functional vinyl monomers together with a large amount of a cross-linking agent and a molecule acting as a template that leaves a kind of memory of its shape and the position of functional groups [1]. Such memory left in the MIP after extraction of the template allows the selective adsorption of the template to the molecular imprints of the MIP. The structural feature of such memory is often described as a cavity having the shape of the template and where the functional groups coming from the functional monomer are favorably positioned and oriented for optimum interaction with the adsorbing template molecules. The cross-linking agent makes the material rigid such that reorganizations that would cause loss of selectivity are prevented.

The choice of the functional monomer is crucial. It is often based on the study of the interactions of the template with the functional monomer, which are either experimentally measured [2] or predicted from theoretical chemistry calculations [3]. Such interactions are generally weak and reversible, leading to a fast kinetic equilibrium between the complex and free molecules. The interactions that actually matter are those with the polymer better than those with the monomers. The relative kinetics of polymerization, the complexation of the template with the growing macromolecules and the organization of imprints within the material during its cross-linking may be of relevance for the formation of molecular imprints. Conventional free radical polymerization (FRP) does not allow for the preparation of well-defined polymers (control of the molar mass of the polymer with time) because the time scale for the growth and termination of a macromolecule is the matter of milliseconds. On the contrary, the use of Radical

Deactivation Reversible Polymerizations (RDRP) slows down the growth of macroradicals by creating dormant species that avoid termination reactions. Until now, it is not clear whether a control of the polymerization kinetics is advantageous for the formation of molecular imprints. Controlled radical polymerization has already been considered for the manufacture of MIPs in several instances since year 2003 [4,5]. Most earlier works only presented the possible implementation of RDRP to MIP manufacture, thereby showing the feasibility. The goals/expectations of RDRP in terms of MIP performance have not been precisely introduced. The outcomes of such experimental work are often improved performance in terms of binding affinity and capacity [4], though their nature and their physicochemical origin are not clearly established. It has often been argued that RDRP could improve MIP performance because the distribution of cross-linking nodes was more homogeneous throughout the material than for FRP [4,5,6]. Indeed, selectivity is related to the cross-linking density and a more homogeneous distribution of cross-linking nodes throughout the polymer materials may lead to a more homogeneous distribution of molecular imprints and a better selectivity of adsorption [7]. As far as we know, such claim of homogeneous distribution of cross-links did not receive direct experimental evidence from structural investigations (e.g. light or X-ray scattering). Kinetics of copolymerization of the mono-functional monomer and cross-linker provide indirect clues of a homogeneous distribution of cross-links. Thus, the experimental kinetics agrees with a random distribution of monomer and cross-linker and a hindered reaction of the pendent vinyl groups that cause cross-linking [8]. The consequence is less intramolecular cross-linking (cyclization) than in FRP. Another consequence is a high efficiency of the cross-linker for binding macromolecules together [9]. It has been argued that the slow propagation rate of RDRP allows the relaxation (reorganization to equilibrium) of macromolecular chains during the polymerization whereas fast FRP causes the formation of heterogeneous materials with microgel domains [10]. In RDRP, gelation takes place at a conversion close to the theoretical gelation threshold whereas FRP causes early onset of gelation. In the presence of a porogen, it has been shown that delayed gelation during RDRP allows phase separation between the cross-linked polymer and the porogen by spinodal decomposition with a homogeneous distribution of pores [11]. Besides cross-linked polymer materials, RDRP allows for the grafting of polymers onto solid surfaces by means of either the “grafting from”, the grafting through and the “grafting to” techniques [12]. This is a definite benefit for applications to chemical sensors that the surface of the transducer is sensitized by functionalization, preferably by means of chemical grafting. This is also useful for applications to capture by selective adsorption because it is easier to optimize the accessibility to the molecular imprints by selecting a favorable morphology of the solid support than by controlling the porosity of the polymer material during the MIP synthesis process [13].

Comparison of MIPs prepared by RDRP and FRP mostly rely on experimental adsorption isotherms of MIP and the corresponding non-imprinted polymer (NIP) showing an enhancement of adsorption for the MIP [4,14,15]. This is indeed the usual way to show an evidence of the presence of molecular imprints in the MIPs. Such an approach restricted to experimental observations does not provide information on the affinity of molecular imprints for the target molecules and the density of molecular imprints. Interestingly, a team from the Nankai University went beyond simple observations by an analysis of adsorption isotherms through Scatchard plots providing the binding constants and density of molecular imprints [16,17,18]. Their material behave quite differently of those reported in many other instances, as it did not show an enhanced adsorption for the RDRP compared to FRP. The Scatchard plots showed that both the binding constant and density of molecular imprints were identical for FRP and the RDRP (either ATRP or RAFT). RDRP processes that have been considered are ATRP, RAFT and iniferter mediated polymerization. Nitroxide mediated polymerization has been investigated in one instance only [14].

The present paper addresses these open questions by comparing the formation of molecular imprints of MIPs manufactured by means of free radical polymerization (FRP) and Radical Deactivation Reversible Polymerization by means of nitroxide-mediated polymerization (NMRP). The selectivity of adsorption and the comparison with the “FRP” one are investigated in a quantitative way through a thermodynamic study of adsorption isotherms.

The synthetic procedure involves the use of methacrylic acid (MAA) as monomer and ethylene glycol dimethacrylate (EGDMA) as the cross-linking agent in the presence of silica as the inorganic support and a small amount of styrene (10 %) to ensure a better control of the MAA polymerization [19,20,21,22,23]. The obtained polymer material is then a cross-linked terpolymer of these three monomers. The model template molecule is 3,5-dichloro-2-hydroxyacetophenone (DCHA), a chlorinated degradation product of the widely used sunscreen octyl methoxycinnamate (OMC). Indeed, photodegradation of OMC in chlorinated waters of swimming pools (containing sodium hypochlorite) yields 2,4-dichlorophenol (DCP), 4,6-trichlorophenol (TCP), 3,5-dichloro-2-hydroxyacetophenone (DCHA) and methoxycinnamic acid (AMC). Owing to its high concentration in environment, DCHA is the main photoproduct of OMC [24]. DCHA is extremely harmful to humans and animals [25]. This hydrophobic organic degradation product can penetrate tissues, reach the bloodstream and cause endocrine disorders [26]. It has been shown that DCHA can accumulate in groundwater through wastewater up to a concentration in the range of few $\mu\text{g}\cdot\text{L}^{-1}$ [27]. Therefore, monitoring the concentration and elimination processes of trace amounts of these degradation products by high

performance liquid chromatography (HPLC) requires an extraction step of compounds from real samples taken in the environment. This latter step is the major source of error in all analysis methods. Solid phase extraction (SPE) using MIP materials is an efficient technique for the purification by means of uptake by selective adsorption [28].

1. Experimental section

1.1. Reagents

Aerosil 200 fumed silica of mean particle size 12 nm and specific surface area $200 \text{ m}^2 \cdot \text{g}^{-1}$ was obtained from Sigma-Aldrich. 3-(trimethoxysilyl)propyl methacrylate (MPTS, 98%), *N*-ethyl-diisopropylamine (DIEA, 98 %), methacrylic acid (MAA, 99%), styrene (S, 99.0 %), 2,2'-azobis-(isobutyronitrile) (AIBN), ethylene glycol dimethacrylate (EGDMA), 2,4-dichlorophenol (DCP, 99 %), 2,4,6-trichlorophenol (TCP, 99 %) and 3,5-dichloro-2-hydroxyacetophenone (DCHA, 99 %) were purchased from Sigma-Aldrich. Toluene (99 %), methanol (99.7 %) and 1,4-dioxane (99 %) were used as received without further purification. Deuterated dimethylsulfoxide (DMSO- d_6) for NMR experiments was purchased from Eurisotop (Saint-Aubin, France).

1.2. Methods

A Perkin Elmer type and a series II model CHS Analyzer 2400 was used for carbon elemental analyses. UV-vis absorbance spectra of DCHA and interfering molecules solutions were recorded using a Perkin-Elmer Lambda 2 UV-Vis spectrophotometer. FTIR measurements in Attenuated Total Reflectance mode (ATR) were performed with a Bruker Alpha FTIR using 24 scans under a 4 cm^{-1} resolution. Liquid state ^1H NMR spectra, and solid-state ^{13}C and ^{29}Si NMR spectra were recorded at 500.13 MHz, 125.76 MHz and 130.32 MHz, respectively on a Bruker Avance III 500 ultra-shield Plus spectrometer. 2D NOESY ^1H - ^1H correlation spectra were run using the noesygpph sequence from the Bruker library with the following acquisition parameters: 90° pulse width = 9.8 μs , spectral width = 4800 Hz (giving an acquisition time of 0.2 s), mixing time = 800 ms, relaxation delay = 1 s. ThermoGravimetric Analysis (TGA) was performed on a Thermal Analyzer Instrument (TA, Q500) in the temperature range from 25 to 800 $^\circ\text{C}$ at a heating rate of $10 \text{ }^\circ\text{C} \cdot \text{min}^{-1}$ under helium atmosphere. A Malvern Zetasizer 3000 instrument was used for measurements of particle sizes by dynamic light scattering and zeta potentials at different pH values on aqueous suspensions of PMAA-*co*-PS, MIPs, NIPs and fumed silica. The full adsorption and desorption isotherms of nitrogen gas were measured at 77 K by the BET method using a Micromeritics ASAP2020 instrument, giving the specific

surface area and mesoporosity. The samples were dried at 150 °C before nitrogen adsorption measurements. The BET specific area was determined by fitting the BET theoretical isotherm to the experimental adsorption branch between the relative pressures p/p_0 0.05 and 0.3. The distribution of porous volume in the mesopores range was determined from the experimental desorption branch by the BJH method. Transmission Electron Microscopy (TEM) images were obtained using a Philips CM120 microscope operating at 80 kV acceleration voltage at the “Centre Technologique des Microstructures” (CT μ) facility of the University of Lyon 1 (<http://microscopies.univ-lyon1.fr/>). A drop of 0.2 % aqueous dispersion was deposited on a Formvar film-coated grid and dried in the open air before TEM observation.

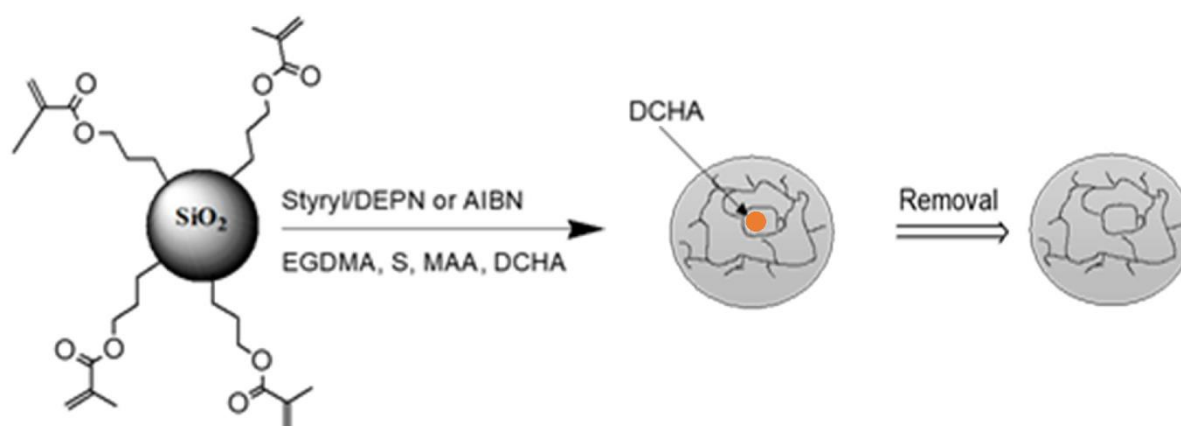
1.3. Grafting of MPTS onto silica nanoparticles

The schematic synthesis of SiO₂-MPTS is shown in Schemes S1, S2 and S3 in Supporting Information. Grafting of MPTS onto silica nanoparticles was performed using three different solvents: Anhydrous toluene, acetone/H₂O and MeOH/H₂O (Table S1). 1 g of silica was dispersed by vigorously stirring in solvent (50 mL) and 3-(trimethoxysilyl)propyl methacrylate was added dropwise to the mixture, followed by the addition of *N*-ethyl-diisopropylamine. The reaction mixture was heated at reflux temperature of the corresponding solvent during 24 h. The resulting products SiO₂-MPTS were washed three times with the reaction solvent, with THF and finally centrifuged at 3500 rpm for 15 min to remove free MPTS. The silica particles functionalized by MPTS were recovered and dried at 40 °C under vacuum. They were stored at ambient temperature for subsequent uses.

1.4. Polymerization processes in the presence of modified silica

The molecular imprinted polymers (MIPs) and non-imprinted polymers (NIPs) were prepared using nitroxide-mediated controlled radical polymerization (NMCP) and by conventional free radical polymerization (FRP) of methacrylic acid. Imprinted polymer MIP-NMCP and non-imprinted polymer NIP-NMCP were synthesized using *N*-tert-butyl-N-[1-diethylphosphono-(2,2-dimethylpropyl)]nitroxide (Styryl/DEPN) as initiator, which was prepared as reported in the literature [29,30]. SiO₂-MPTS (1 g) was dispersed in 1,4-dioxane (15 mL) in a Schlenk flask. Then, methacrylic acid (0.020 mol, 90 %), styrene (0.002 mol, 10 %), ethylene glycol dimethacrylate (0.011 mol, 45 %) and DCHA (0.0025 mol) were added. After 10 min stirring, Styryl/DEPN (10 wt% relative to styrene monomer) was introduced into the mixture to control the polymerization reaction [22]. The mixture was degassed by 4 freeze-thaw cycles and heated in an oil bath at 110 °C. The resulting material was filtrated and washed with the same solvent

to eliminate the free polymer chains. Finally, DCHA was eliminated from the silica-based material by using a Soxhlet extractor with methanol as solvent for 48 h and then dried under vacuum at 40 °C. Non-imprinted polymers were synthesized using the same protocol without DCHA and submitted to the same extraction process. In order to compare materials prepared by NMRP and FRP, homologues MIP-FRP and NIP-FRP were synthesized by FRP under the same experimental conditions as NMRP, but using AIBN as an initiator. The synthesis of MIPs and NIPs sorbents are schematically presented in [Scheme 1](#).



Scheme 1. Synthesis of molecular imprinted polymers using radical polymerization.

1.5. Characterization of template-monomer interactions

¹H NMR spectra of mixtures of DCHA at a constant concentration (78 mM) in DMSO-*d*₆ and MAA at varying concentrations in the range of 233 mM to 930 mM in DMSO-*d*₆ were recorded at 25 °C to assess the interactions between DCHA and MAA. Then, the DCHA and MMA solutions were mixed together by stirring them during 10 min to ensure the formation of the pre-polymerization complex. The chemical shifts of DCHA protons (HA, HB, HC) were measured as a function of the increasing concentration of MAA.

1.6. Adsorption studies

The adsorption of DCHA onto MIPs or NIPs was studied in batch experiments where 30 mg of material was immersed in 5 mL of DCHA solutions of different concentrations C_0 ranging from $2.4 \cdot 10^{-5} \text{ mol}\cdot\text{L}^{-1}$ to $10^{-4} \text{ mol}\cdot\text{L}^{-1}$. After an equilibration time, the samples were centrifuged and the residual concentration C of the supernatant was measured using UV-vis absorbance spectroscopy. The adsorbed amount Q ($\text{mol}\cdot\text{g}^{-1}$) and the percentage of adsorption (%*A*) were calculated according to the following equations [\[31,32\]](#)

$$Q = \frac{(C_0 - C)V}{m} \quad (\text{eq. 1})$$

$$\%A = \frac{(C_0 - C)}{C_0} \times 100 \quad (\text{eq. 2})$$

where V (L) is the volume of the solution, m (g) is the mass of MIP or NIP, C_0 and C ($\text{mol}\cdot\text{L}^{-1}$) are the initial and equilibrium concentrations of DCHA in solution, respectively.

The imprinting factor was calculated as [33]:

$$IF = \frac{Q_{\text{MIP}}}{Q_{\text{NIP}}} \quad (\text{eq. 3})$$

where Q_{MIP} and Q_{NIP} respectively stand for the equilibrium adsorption capacity of MIP and NIP adsorbent.

2. Results and discussion

2.1. Molecular imprinted nanomaterials

The preparation procedure of imprinted nanomaterials MIP and NIP (Scheme 1) requires two steps: (i) modification of the silica surface to provide anchored methacrylic monomers that can be used for subsequent copolymerization (ii) grafting molecular imprinted polymer onto the silica surface using both conventional free radical copolymerization and nitroxide-mediated radical polymerization. Firstly, two processes were studied for attaching MPTS silane onto the silica surface: the anhydrous process and the wet process. The former anhydrous process involves a direct reaction of methoxysilyl groups with surface silanol groups leading to a dense monolayer of silane (Scheme S1). In the wet process, the hydrolyzed silane in acetone/water or methanol/water as solvents reacts with silanols groups of silica nanoparticles by a condensation reaction [34]. The wet process allows the formation of a thick layer of polysiloxane by polycondensation of the organosilane at the silica surface (Schemes S2 and S3). The characterization of the MPTS-grafted silica is presented in Supporting Information. In all cases, MPTS was successfully grafted onto the silica surface. The highest grafting density was reached using the wet process in acetone/water and methanol/water solvents. The MPTS grafting density obtained when using anhydrous toluene as solvent varied from 2.1 to 2.4 $\mu\text{mol}\cdot\text{m}^{-2}$, depending on the amount of the initial MPTS (Table S1). The silica surface coverages by grafted other methacrylate-based alkoxy-silanes were in the same range as that previously achieved under the same conditions [35,36]. This latter experimental protocol, yielding a silica coated by a dense monolayer of grafted silane, was selected for the preparation of the solid support of imprinted materials.

2.2. Detection of template-monomer interactions in the pre-polymerization medium

Interactions between the target molecule and the monomer have been assessed by ^1H NMR spectroscopy [37,38]. ^1H NMR spectra of DCHA with different concentrations of MAA monomer in $\text{DMSO-}d_6$ solution were recorded to evaluate pre-polymerization mixtures and to determine the most suitable MAA/DCHA ratio for the preparation of MIP. The comparison of ^1H NMR spectra at various MAA/DCHA molar ratios (from 3 to 8) with the corresponding pure DCHA revealed noticeable chemical shift variations (Figure 1 and Table S2). All DCHA protons (HA, HB and HC) showed a shift to high field in the presence of MAA. The largest shift was observed for HB protons in ortho position to the carbonyl group. This is suggesting the formation of hydrogen bonds between the DCHA carbonyl groups and the MAA carboxylic acid functions. The chemical shifts were increasing with respect to DCHA/MAA ratio increasing from 3 to 8. This is indeed trivial that more MAA causes the formation of more complex species. However, a large amount of the monomer is concomitant with a low amount of cross-linker and a poor freezing of molecular imprints by cross-linking. The consequence of an excessive amount of MAA would be an increase of non-specific interactions. Conversely, a small amount of MAA would cause a low density of specific recognition sites. A compromise has been decided at MAA/DCHA molar ratio of 8/1. The most used range of DCHA/MAA molar ratio is indeed in the range 4/1 to 16/1 in the case of non-covalent interactions because it has often led to better selectivity of the MIP [13,39,40].

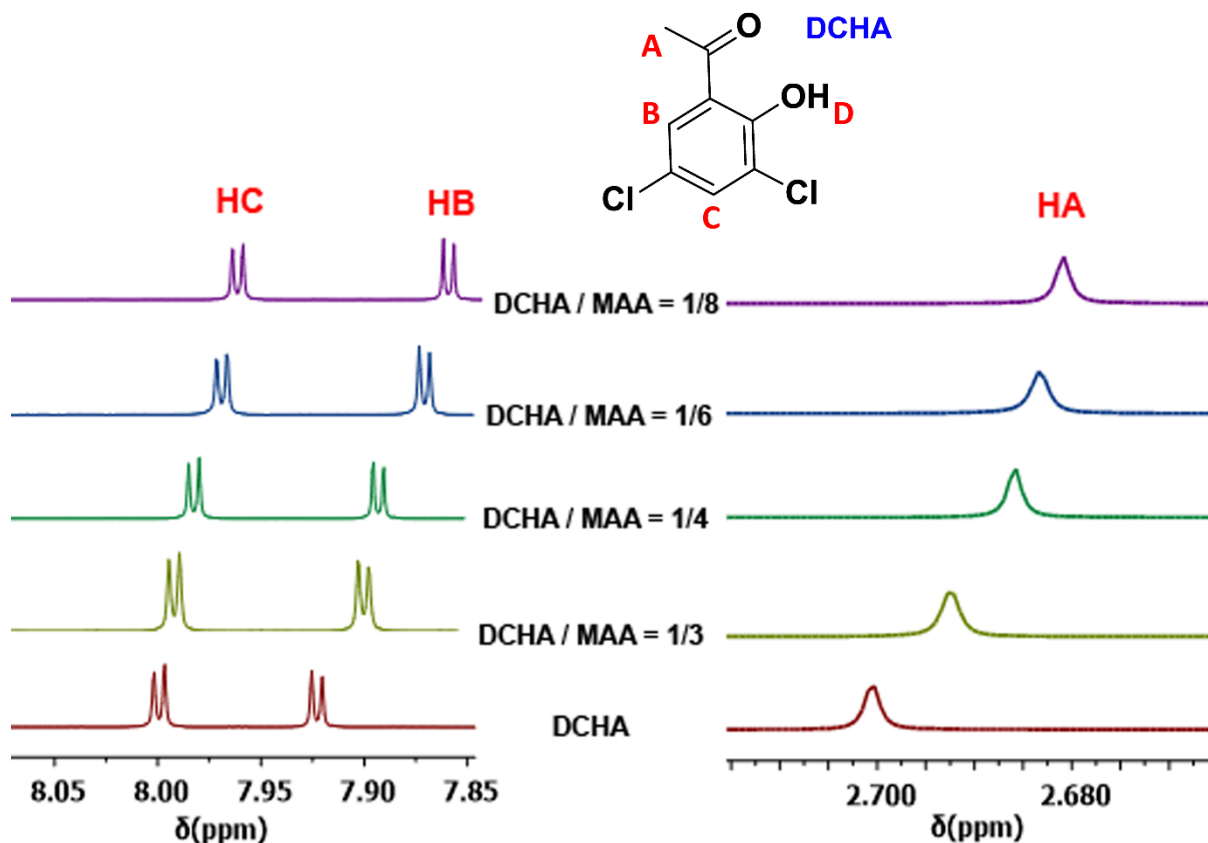


Figure 1. ^1H NMR spectra of DCHA at a constant concentration of $7.8 \cdot 10^{-2} \text{ mol}\cdot\text{L}^{-1}$ in the presence of several concentrations of MAA: pure DCHA, and mixed DCHA/MAA at molar ratio of 1/3, 1/4, 1/6 and 1/8 in $\text{DMSO-}d_6$.

In addition, the NOESY 2D NMR technique allowed confirmation of the DCHA/MAA interaction. Indeed, correlation peaks are detected for all protons of DCHA and MAA in the 2D NOESY contour plot for a DCHA/MAA molar ratio of 1/8 (Figure 2). The most intense correlation peaks appeared between HC protons of DCHA and both HE and HG protons of MAA, indicating the close proximity of all these protons. The presence of a strong correlation peak between HC and HG showed that the vinyl part of MAA was close to the phenyl group of DCHA, whereas the carboxylic acid group of MAA was hydrogen-bonded to the carbonyl group of DCHA. The correlation peaks between HB and MAA protons were weaker, showing that the position of MAA in the complex species was shifted towards the Cl–C–C–OH side of the aromatic ring of DCHA with its –COOH group and HG proton in cis position being closer to the DHCA phenyl ring. This tentative structure of the complex is consistent with the establishment of a supplementary interaction of the DCHA phenyl and MAA vinyl groups by means of Π -stacking.

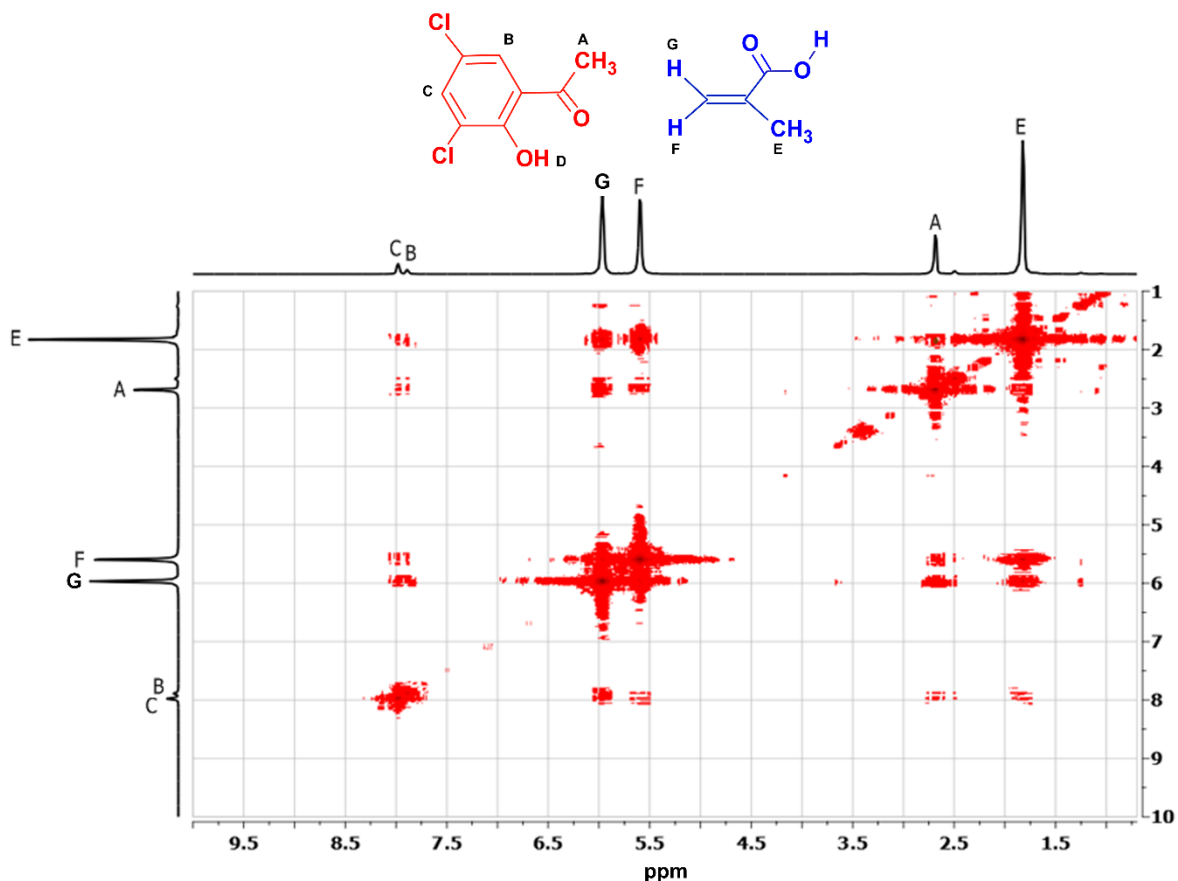


Figure 2. 2D NOESY spectrum of DCHA/MAA mixed solution in DMSO- d_6 at a 1/8 molar ratio.

2.3. Preparation of imprinted polymers by nitroxide-mediated and conventional free radical polymerization

The syntheses of imprinted and non-imprinted poly(methacrylate-*co*-styrene) polymers immobilized on silica surface were done by two synthetic methods using nitroxide-mediated radical polymerization (NMRP) and free radical polymerization (FRP). As discussed by Charleux et al. [19,20,21], the main difficulty in the control of the polymerization of methacrylic monomers by nitroxides is related to the very high activation-deactivation equilibrium constant, K , which prevents the use of SG1/DEPN-mediated polymerization to achieve the synthesis of living homopolymers. In order to decrease the activation-deactivation equilibrium constant, a small amount of styrene was added into the MAA polymerization media. Moreover, no chain transfer reaction to the solvent was observed when using 1,4-dioxane or ethanol. The detailed mechanistic discussion has been given for methyl methacrylate [19,20,21] and the specific instance of methacrylic acid monomer has been given latter [22,23]. Therefore, a small amount of styrene comonomer (10 %) was added to the reaction medium to slow down the MMA propagation rate, resulting in a more efficient radical scavenging by the

nitroxide. The main objective is comparing the formation of molecular imprints through NMRP and FRP. The MIPs materials MIP-NMRP and MIP-FRP were prepared through the copolymerization of grafted methacrylate groups of SiO₂-MPTS and MAA monomer and EGDMA cross-linker added in the polymerization reaction medium in presence of DCHA in a non-polar organic solvent, respectively using either Styryl-DEPN and AIBN as initiator. It was demonstrated that DCHA establishes strong interactions with MAA at a 1/8 molar ratio, as mentioned in the previous section. NMRP is performed at high temperature (110 °C) to activate dormant Styryl/DEPN-based species, while the AIBN initiated radical polymerization initiator allows the fast polymerization of MAA at 70 °C (Scheme 1). The MIP and NIP materials were characterized by IR spectroscopy, solid-state ¹³C CP-MAS NMR, TGA and elemental analyses of carbon.

The infrared spectra of SiO₂-MPTS, MIP-NMPPR and NIP-NMPPR, presented as absorbance-normalized using the strong band of SiO₂ at 1100 cm⁻¹ (Figure 3), confirmed the binding of the polymer material to SiO₂-MPTS after the polymerization step. IR spectra showed that DCHA has been removed to completion from the MIP-NMPPR during the extraction step because there was no difference between the spectra of MIP and NIP, and IR bands pertaining to DCHA were not visible in the spectra of the MIP, in particular those at 553 and 637 cm⁻¹ appearing in a clear region of the MIP spectrum. The comparison of IR spectra of MIP-NMPPR and NIP-NMPPR to SiO₂-MPTS revealed a large increase in intensity of the carbonyl band of ester groups at 1750 cm⁻¹ because of an additional ester group brought by EGDMA, as well as the increase in intensity of the bands of the C–H stretching vibrations at 2900–3000 cm⁻¹ because of the presence of the organic polymer shell. Solid-state ¹³C CP-MAS NMR spectra of MIP-NMRP and NIP-NMRP (Figure S4 in Supporting Information) displayed the expected peaks of the MAA-*co*-EGDMA copolymer, showing the successful polymerization. There was no noticeable difference between the solid-state ¹³C spectra of MIP and NIP, in agreement with expectations.

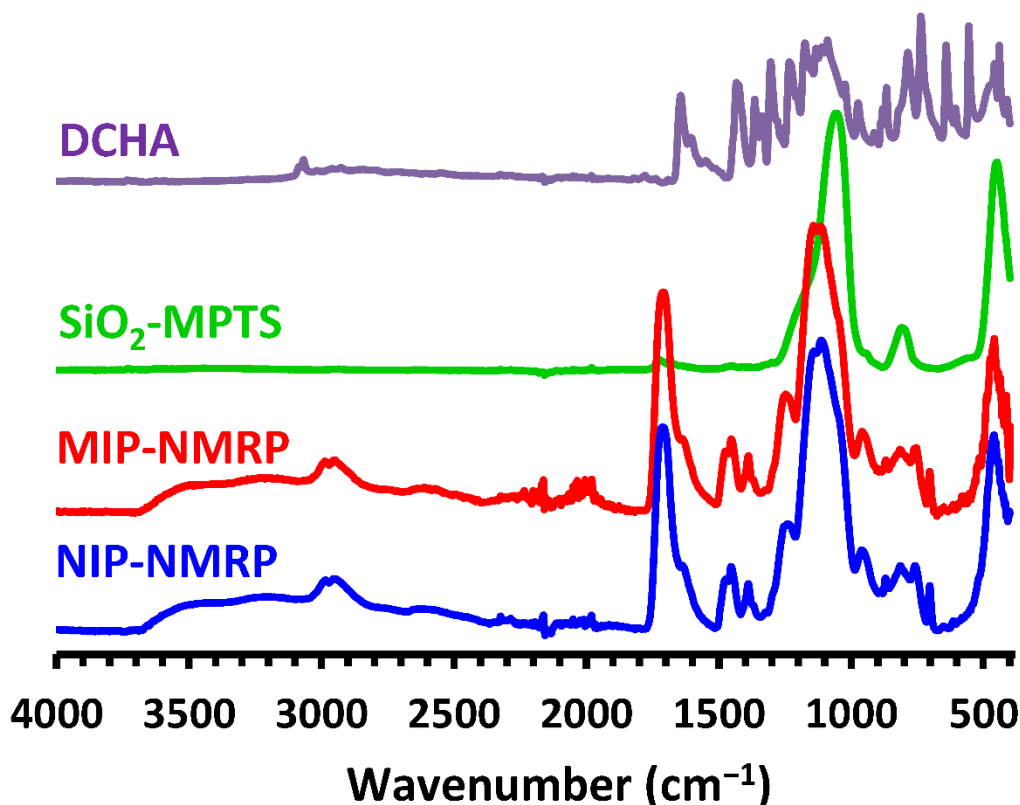


Figure 3. IR spectra of DCHA, SiO₂-MPTS, MIP-NMRP and NIP-NMRP.

Then, quantitative determinations of polymer content were performed by TGA and elemental analysis of carbon (EA). Similar TGA results were observed for MIP and NIP (Figure S4 in Supporting Information). The differences polymer contents of all samples inferred from TGA were less than 3 %. The detailed interpretations of TGA and elemental analysis in terms of polymer content are given in Supporting Information. Elemental analyses and TGA were in close agreement. Owing to the small differences of mass losses and elemental analyses of carbon, the mass fractions of polymer of all samples are close each other (Table 1). A mean value is 90 %.

Table 1. Mass fractions of polymer in the MIPs and NIPs determined by TGA and elemental analysis of carbon.

Materials	Mass loss (%) 200–600 °C	Elemental analysis (%)	Polymer content (g g ⁻¹)	
			from TGA	from EA
MIP-NMRP	89.2	50.8	0.903	0.892
NIP-NMRP	90.7	51.4	0.914	0.907
MIP-FRP	88.2	51.2	0.910	0.882
NIP-FRP	90.0	50.2	0.892	0.900

Assuming a core–shell morphology of the material as a core of silica coated by grafted polymer, a ‘grafting density’ ($\text{g}\cdot\text{m}^{-2}$) and a mean thickness of the polymer coating were calculated from the mean mass fraction of polymer, the density of the polymer and the specific surface area of silica ($200 \text{ m}^2\cdot\text{g}^{-1}$). Because the density of the polymer was not known, the density of the 50:50 copolymer of methacrylic acid and ethyl acrylate (Eudragit® L 100-55) was taken as an estimate: $\rho = 0.83 \text{ g}\cdot\text{cm}^{-3}$ [41]. Using the latter value, the resulting mean thickness is calculated to be 50–60 nm, which is much larger than the mean diameter of silica primary particles of Aerosil 200 fumed silica. The core–shell morphology with each primary silica particle being encapsulated by a polymer shell is not realistic on this basis. A more complex morphology has been disclosed by TEM observations.

The morphology of the materials prepared by NMRP and FRP has been characterized by means of TEM observations and DLS measurements. An outcome of both techniques was the mean size of particles (Figure 4). TEM pictures of MIP-FRP material showed particles with quite a broad distribution of sizes in the range 100–500 nm (Figure 4A). The size distribution of MIP-NMRP material (Figure 4B) distinctly showed a narrower size distribution. Both materials contain very small silica particles buried inside them; they are clearly visible as dark spots on the TEM pictures at high magnifications on the right hand side of Figures 4A and 4B. The MIP-NMRP and MIP-FRP materials are composites made of a polymer matrix with silica particles included inside them. An image analysis of TEM pictures yielded a number-averaged particle size of 210 nm with a standard deviation of 150 nm for FRP and a mean particle size of 250 nm with a *SD* of 40 nm for the population of large particles of NMRP material. The difference of mean sizes is not significant owing to the small number of particles taken for the calculation ($p = 0.24$ in a Student *t*-test of unequal variance). Conversely, the difference of distribution width expressed by the standard deviation makes sense ($p = 0.007$): the size distribution of FRP is much broader than that of NMRP.

DLS measurements provided the distribution of hydrodynamic diameter of MIP-NMRP and MIP-FRP particles (Figure 4C). The population of small particles of MIP-NMRP material could not be detected by DLS because of the presence of the other population of larger particles. The mean size of MIP-NMRP was smaller than MIP-FRP. The particle size distribution of MIP-NMRP and MIP-FRP were in the range 150–200 nm and 100–700 nm, respectively. The particle sizes measured by DLS were much larger than from TEM. Indeed, DLS measurements are performed on particles dispersed in water, whereas TEM observations are done with dry particles. The larger particle sizes measured by DLS revealed an extensive swelling of particles by water. MIP-FRP particles are swollen to a higher extent than MIP-NMRP particles. The

narrower particle size distribution and lesser swelling may be related to the formation of a more homogeneous network of cross-linked polymer by NMRP [42].

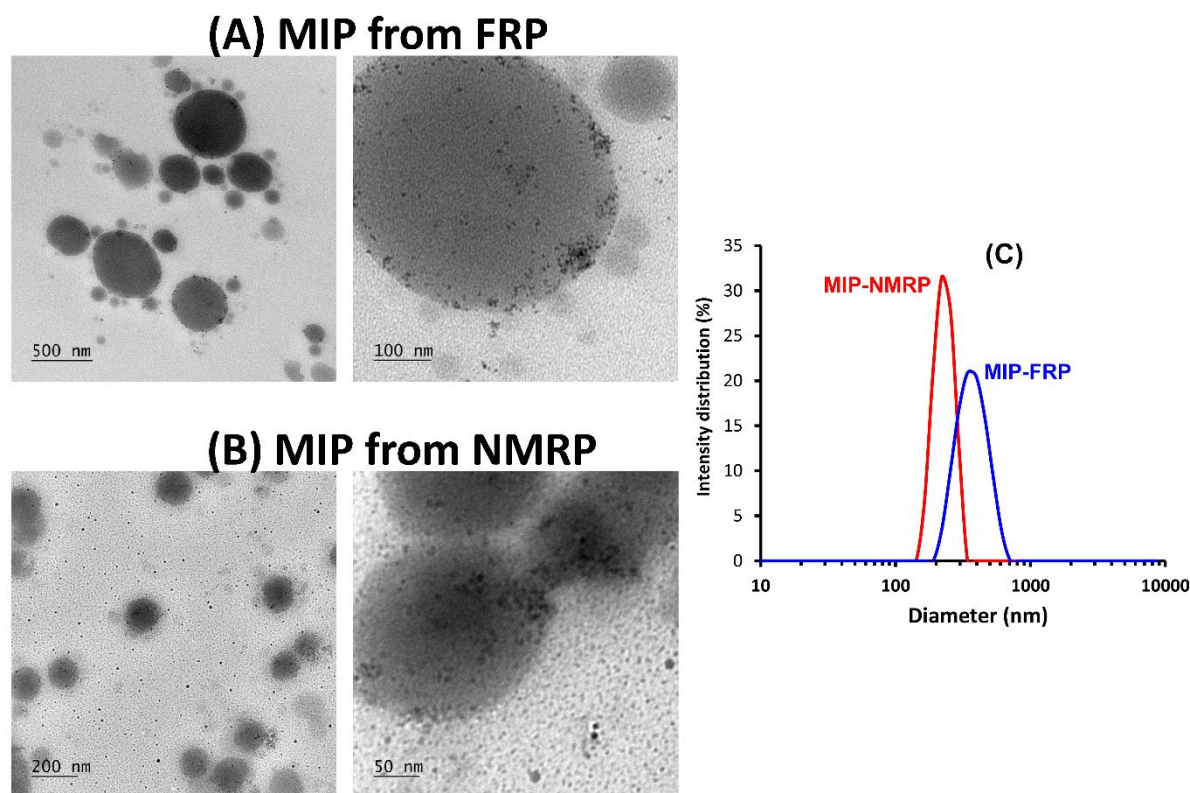


Figure 4. TEM images MIP-FRP (A) and MIP-NMRP (B) at two magnifications and particle size distribution from DLS (C).

The specific surface area and porosity of the materials were assessed by means of BET measurements of nitrogen gas adsorption at 77 K (Figure 5A). The adsorption isotherms of MIP-FRP and MIP-NMRP were of the type IV showing a hysteresis between the adsorption and desorption branches. The BET specific surface area was $A_{SP} = 14 \text{ m}^2 \cdot \text{g}^{-1}$ for the MIP-FRP and $A_{SP} = 17 \text{ m}^2 \cdot \text{g}^{-1}$ for the MIP-NMRP. These were much lower than that of the silica solid support, confirming the conclusion previously reached that the material does not have a core-shell morphology made of a silica core coated by the MIP material. A mean diameter of the particles assuming a spherical shape was calculated as $\langle \text{Diam} \rangle = 6/\rho A_{SP} = 500 \text{ nm}$ (with the density of the polymer material taken as $\rho = 0.83 \text{ g} \cdot \text{cm}^{-3}$). The mean diameters were $\langle \text{Diam} \rangle = 500 \text{ nm}$ for the MIP-FRP and $\langle \text{Diam} \rangle = 400 \text{ nm}$ for the MIP-NMRP, in agreement with the DLS measurements. The size distribution of the mesopores assessed from the BJH analysis of the desorption branch showed a low porous volume with a mean pore size of 10 nm for both

materials (Figure 5B). The total (cumulated) mesoporous volume was $0.05 \text{ cm}^3 \cdot \text{g}^{-1}$ ($\sim 5 \%$) for the MIP-FRP and $0.06 \text{ cm}^3 \cdot \text{g}^{-1}$ ($\sim 6 \%$) for the MIP-NMRP, which showed that the materials were essentially non-porous.

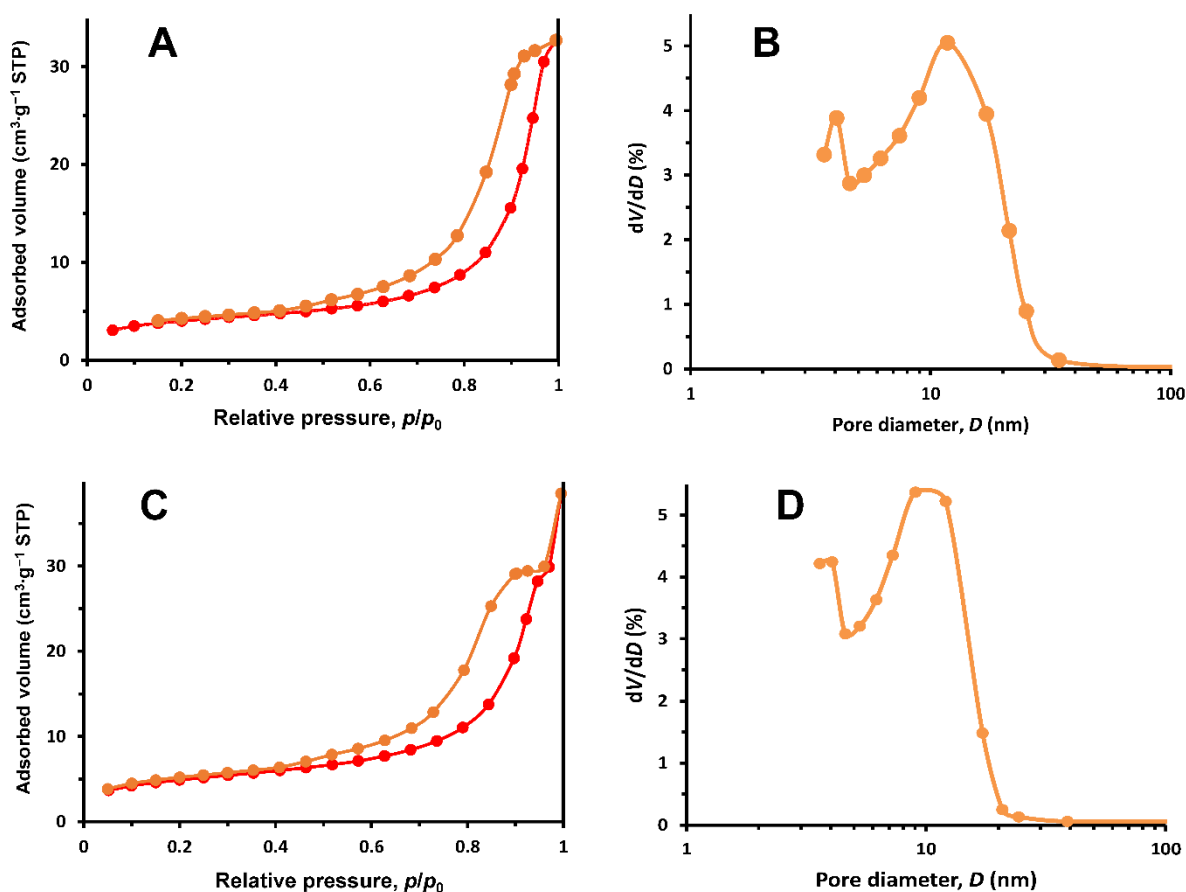


Figure 5. Adsorption (red) and desorption (orange) isotherms of nitrogen gas at 77 K onto the MIP-FRP material (A) and the MIP-NMRP material (C). Distribution of the mesoporous volume assessed by application of the BJH method to the desorption branch for the MIP-FRP (B) and the MIP-NMRP (D).

The pH has an important role in adsorption processes because it influences the charges of molecules in solution and the surface charge of the adsorbent. Zeta potentials of MIP-NMRP and NIP-NMRP were measured as a function of pH to determine their isoelectric point (*iep*) and thereby infer the role of surface charge of the adsorbent on DCHA binding. The zeta potential curves of the MIP-NMRP and NIP-NMRP (Figure 6) exhibit similar behavior; the *iep* was 4.1 for both MIP-NMRP and NIP-NMRP. This value of *iep* is very different of that of bare fumed silica (2.0), and in agreement with the *iep* of 4.1 measured for the bulk cross-linked

(PMAA-*co*-PS) material prepared in the same experimental conditions in the absence of silica. Such results confirmed that the silica particles were buried inside the polymer and the outer surface of these materials was made of PMAA-*co*-PS. The surface charge of both MIP-NMRP and NIP-NMRP materials is positive for pH < 4 and negative for pH > 4.

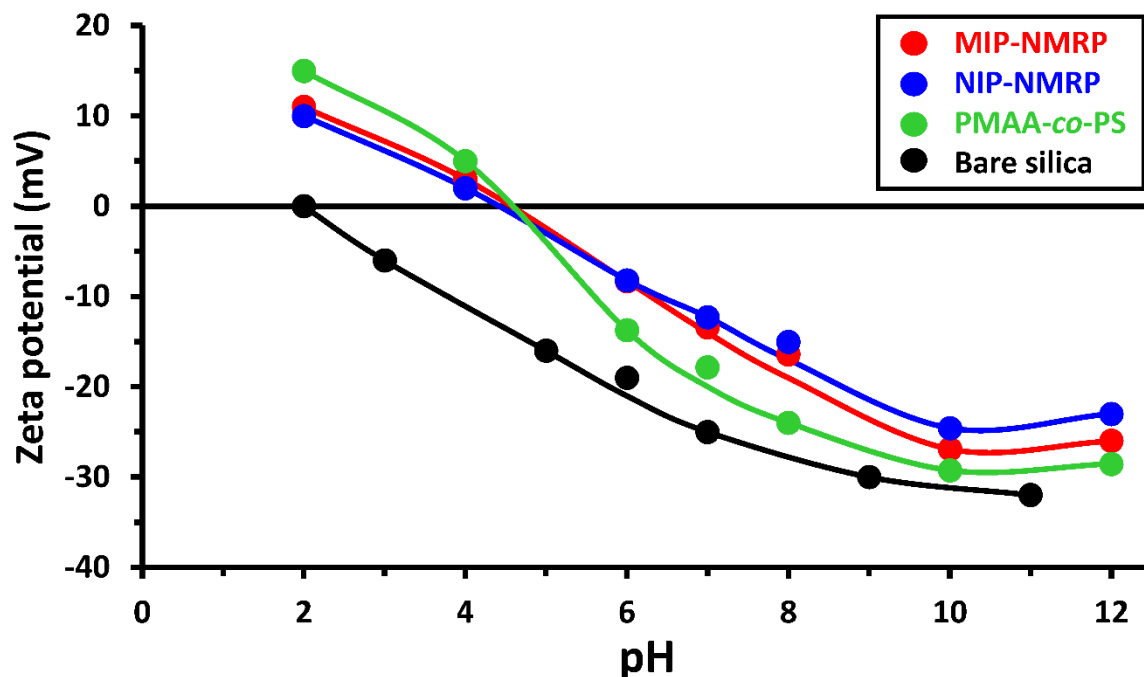


Figure 6. Zeta potential of MIP-NMRP (red), NIP-NMRP (blue), PMAA-*co*-PS (green) and non-modified silica (black) at different pH.

2.4. Performance for adsorption of DCHA

The adsorption efficiency of DCHA depends on the surface charge of materials that varies with respect to pH (Figure 7A). The highest adsorption capacity of MIP-NMRP from a DCHA solution with a concentration of $2.42 \cdot 10^{-5} \text{ mol}\cdot\text{L}^{-1}$ (76 %) was reached at pH 7. The adsorption capacity decreases in more acidic and basic media. Under all pH conditions, the adsorption capacity of MIP-NMRP is higher than that of NIP-NMRP, showing the formation of molecular imprints in MIP-NMRP.

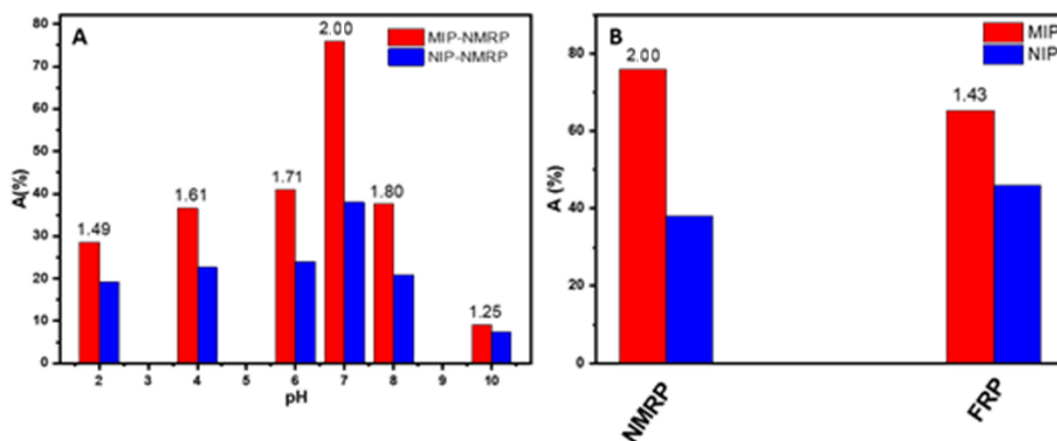


Figure 7. (A) Adsorption capacity of MIP-NMRP and NIP-NMRP at $C = 2.42 \cdot 10^{-5} \text{ mol}\cdot\text{L}^{-1}$ at different pH. (B) Adsorption capacity of MIP-NMRP and MIP-FRP for $C = 2.42 \cdot 10^{-5} \text{ mol}\cdot\text{L}^{-1}$ at pH = 7. Numbers given on top of each bar are imprinting factors.

Owing to the pK_a of DCHA (8.26), DCHA can be considered as a neutral molecule below $\text{pH} = pK_a - 2 = 6.3$; and it turns more and more negatively charged as pH increases because of the deprotonation of its phenol group. There is an obvious electrostatic contribution to the adsorption of DCHA and it should be the same behavior for MIP and NIP and for NMRP and FRP materials. Both the polymer materials and DCHA are negatively charged at basic pH, so that the adsorption to both MIP and NIP are very low at pH 10. At pH 7 for which there is maximum adsorption, the polymer materials are almost fully ionized and the phenol group of DCHA is 95% under its neutral $\Phi\text{-OH}$ form. The fraction of the neutral $\Phi\text{-OH}$ form drops down to 50% at pH 8.26. The formation of a hydrogen bond between the $\Phi\text{-OH}$ and CO_2^- groups is favorable at this pH and in the pH range 4–8.26. The contribution of such a hydrogen bond provides a rationale for the maximum binding to MIP-NMRP and NIP-NMRP materials at pH 7. The electrostatic contribution is the origin of the dissymmetry of the adsorption behavior at either side of pH 7. Enhanced interactions by hydrogen bonding and/or supplementation by additional interactions are responsible for the higher adsorption of MIP-NMRP material.

The adsorption capacities of NMRP and FRP materials were compared at pH 7 (Figure 7B). The DCHA uptake using MIP-NMRP as adsorbent is larger than MIP-FRP adsorbent, whereas the adsorptions for both NIP materials were almost the same. The latter observation was expected since the interactions of DCHA with the cross-linked PMAA-*co*-PS material in its disordered state are the same. Enhanced adsorption to the MIP with respect to the NIP is due to the favorable position and orientation of functional groups in the molecular imprints as this is

the case for any MIP material. Implementation of NMRP brings a definite benefit regarding the formation of molecular imprints. The exact origin of such benefit is difficult to figure out. It has often been stated as a clue that NMRP yields a more homogeneous distribution of cross-linking points [6]. There is neither evidence of this effect, nor experimental comparative measurements of cross-links distribution. The origin of higher binding to molecular imprints formed by the NMRP process remains an open issue about which a more detailed comparison of adsorption performance through a thermodynamic interpretation of equilibrium adsorption isotherms will bring valuable information.

2.5. Adsorption kinetics

The effect of contact time on DCHA adsorption onto MIP-NMRP and NIP-NMRP at different concentrations of DCHA (from $2.42 \cdot 10^{-5}$ to 10^{-4} mol·L⁻¹) was measured in adsorption kinetics experiments using the depletion method (Figure 8). At all tested DCHA concentrations, the adsorption of DCHA onto MIP-NMRP material was much larger than onto NIP-NMRP during the adsorption equilibration time. Both binding to molecular imprints and non-selective adsorption off the molecular imprints were quite fast processes. Adsorption equilibrium was reached within about 1 h. 50 % uptake occurred within a short time less than 20 min.

The adsorption kinetics to MIP and NIP materials should be different in case of a reaction-controlled adsorption process where the rate-limiting step is the rate at which DCHA molecules close to the surface finally bind to it. Indeed, the adsorption process to the MIP material requires that the DCHA molecule is oriented in the right way for optimum interactions with the functional group of the molecular imprints. Consequently, only part of the contact events of DCHA with the material surface leads to effective binding. On the contrary, adsorption to the surface of NIP materials only requires that the DCHA molecules reach the surface. The curves for the kinetics of MIP-NMRP and NIP-NMRP (Figure 8) are different because the adsorbed amounts reached at equilibrium are different. Upon rescaling the kinetics results by the adsorbed amounts at equilibrium, the behaviors of MIP-NMRP and NIP-NMRP get nicely superimposed. This observation rules out the reaction-limited adsorption process. The rate-limiting step is better the diffusion of DCHA molecules from the bulk solution to the molecular imprints.

The rapid adsorption process for MIP-NMRP could be attributed to a large available surface area of the material. Faster adsorption was observed for molecular imprints in a thin layer of frozen polyaniline (PANI) coating the surface of a silica support [36]. This was achieved

because the mean polymerization degree of PANI strands grafted to the surface was 4, giving a coating mean thickness of 0.7 nm. The size of the benzophenone-4 adsorbing molecule was larger than DCHA, so that its diffusivity was smaller than that of DCHA; diffusion-limited adsorption of DCHA to the PANI-coated silica material would be even faster. In the present case, the structure is better than that of a composite material of cross-linked polymer filled with very small silica particles. The small size of the composite particles (150–200 nm as measured by DLS) allows much faster diffusion to the surface than for porous polymer beads of 10–100 μm size. The present adsorption time-scale is indeed much shorter than the typical time spanning from hours to days [36] for adsorption to beads of imprinted materials prepared by traditional dispersion polymerization in the presence of porogen [43]. Application of MIPs to solid phase extraction (SPE) process for samples purification and pre-concentration indeed requires fast adsorption to allow short duration and high flow rate of analyses.

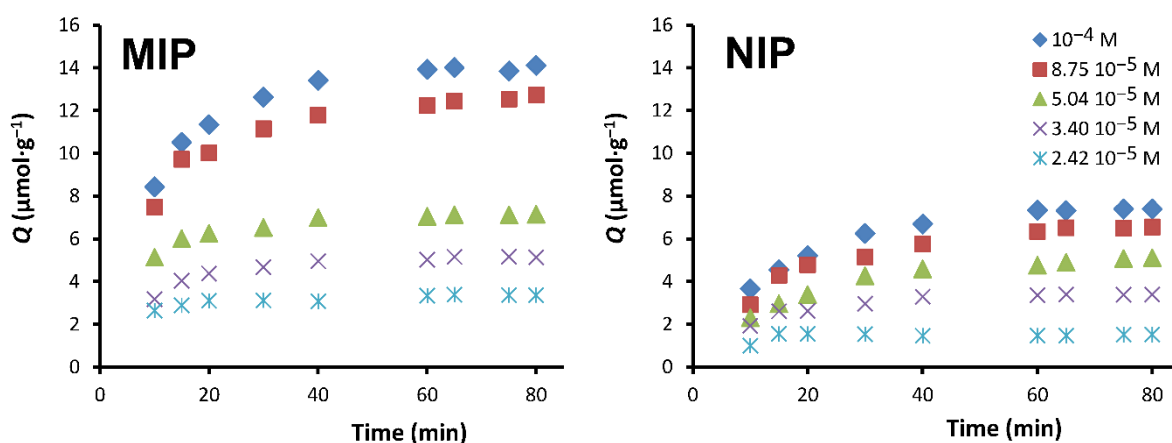


Figure 8. Adsorption kinetics experiments onto MIP-NMRP and NIP-NMRP from DCHA solutions of several concentrations (\blacklozenge): $10^{-4} \text{ mol}\cdot\text{L}^{-1}$, (\blacksquare): $8.75 \cdot 10^{-5} \text{ mol}\cdot\text{L}^{-1}$, (\blacktriangle): $5.04 \cdot 10^{-5} \text{ mol}\cdot\text{L}^{-1}$, (\times): $3.40 \cdot 10^{-5} \text{ mol}\cdot\text{L}^{-1}$ and (\ast): $2.42 \cdot 10^{-5} \text{ mol}\cdot\text{L}^{-1}$.

2.6. Thermodynamics of adsorption

Adsorption thermodynamics have been studied by modeling equilibrium adsorption isotherms with the Volmer and Langmuir–Volmer theoretical models. The Langmuir isotherm is a classical model, which describes adsorption to homogeneous and independent sites on the surface of the adsorbent. The use of this model involves reversible adsorption with identical adsorption energy for all sites. The adsorbed density Q ($\mu\text{mol}\cdot\text{g}^{-1}$) in equilibrium with a solution of concentration C ($\text{mol}\cdot\text{L}^{-1}$) is described by two parameters: the maximum adsorption capacity

Q_{\max} corresponding to density of adsorption sites, and the adsorption equilibrium constant K according to the following expression [44]:

$$Q = Q_{\max} \frac{K C}{1 + K C} \quad (\text{eq. 4})$$

The Volmer model describes adsorption on a surface where there is no defined adsorption sites. In such a case, the adsorbed molecules can freely diffuse on the surface contrary to the Langmuir model. The Volmer equation writes [45]:

$$C = \frac{1}{K} \frac{\theta}{1 - \theta} e^{\frac{\theta}{1 - \theta}} \quad (\text{eq. 5})$$

where θ is the surface coverage, $\theta = Q/Q_{\max}$, and K is the binding constant for adsorption equilibrium. Numerical resolution of eq. 5 written as C versus Q yields the adsorption isotherm Q as a function of C . Thus, the Langmuir model pertains to localized adsorption (on specific sites) whereas the Volmer model pertains to non-localized adsorption where the adsorbed molecules are mobile. The correct model for adsorption to MIPs is a combination of the Langmuir model for localized adsorption to molecular imprints and Volmer model for non-localized adsorption off the molecular imprints. Adsorption to NIPs is also described by the Volmer model. Selective adsorption to molecular imprints is described by the parameters $Q_{\max,s}$ and K_s where the subscript “s” stands for selective. Adsorption on NIPs and off the molecular imprints of MIPs is defined as non-selective (subscript “ns”) considering the mobility of adsorbed molecules; the parameters of the Volmer equation are $Q_{\max,ns}$ and K_{ns} . The adsorption to MIPs is the sum of the selective and non-selective adsorptions; this overall model introduced by Ayadi et al. [36] has been called Langmuir–Volmer.

The Langmuir–Volmer and Volmer models were fitted to the experimental adsorption isotherms of MIPs and NIPs respectively. The outcome is a thermodynamic description of the adsorption process in terms of the parameters Q_{\max} and K for both adsorption to molecular imprints and off the molecular imprints. As an important feature of modeling for comparing adsorption data, it allows discriminating the origin of differences in adsorption data of different materials, in particular NMRP and FRP. Thus, an enhanced adsorption may come from either a larger number of molecular imprints through increased $Q_{\max,s}$, or a higher affinity to adsorption sites through a larger value of K_s .

Experimental adsorption isotherms at 298 K pH 7 and the best fit of the suitable model are given for MIP-NMRP, NIP-NMRP, MIP-FRP and NIP-FRP in Figure 9. The thermodynamic parameters are given in Table 2. Concentrations are expressed in $\text{mol}\cdot\text{L}^{-1}$, so that the values of K (with no unit) correspond to a standard state of $1 \text{ mol}\cdot\text{L}^{-1}$ concentration. The fits of the models

to the experimental data made by minimizing the average relative error ARE (eq. 6 where n is the number of data points and p the number of adjustable parameters) are excellent, showing the adequacy of the models.

$$ARE = \frac{1}{n-p} \sum_{i=1}^n \left| \frac{Q_{\text{exp}} - Q_{\text{calc}}}{Q_{\text{exp}}} \right| \quad (\text{eq. 6})$$

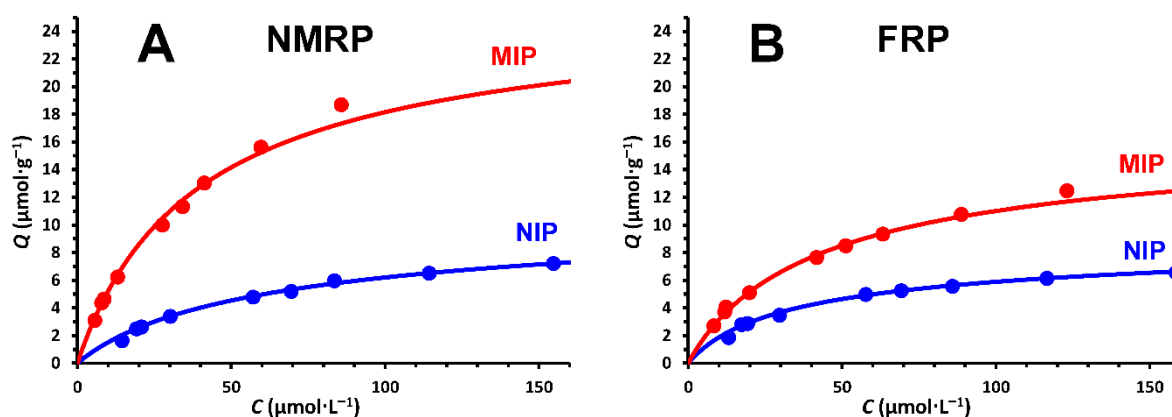


Figure 9. Adsorption isotherms and best non-linear fits of the adsorption models to experimental DCHA adsorption onto MIP-NMRP and NIP-NMRP (A), MIP-FRP and NIP-FRP (B).

Table 2. Parameters of the Langmuir–Volmer and Volmer models fitting to DCHA experimental adsorption isotherms onto MIP-NMRP, NIP-NMRP, MIP-FRP and NIP-FRP at 298 K and pH 7.

	$Q_{\text{max},s}$ ($\mu\text{mol}\cdot\text{g}^{-1}$)	K_s	$\log(K_s)$	$Q_{\text{max},ns}$ ($\mu\text{mol}\cdot\text{g}^{-1}$)	K_{ns}	$\log(K_{ns})$
MIP-NMRP	19.6	25000	4.40	9.0	20000	4.30
NIP-NMRP				16.3	11000	4.05
MIP-FRP	10.5	21000	4.32	9.0	21000	4.33
NIP-FRP				12.7	20000	4.31

As shown in Figure 9, the theoretical adsorption isotherms fit quite well the experimental data in all instances. Adsorbed amounts to MIPs are larger than those of NIPs, showing the presence of molecular imprints in MIP materials prepared by both the FRP and NMRP processes. The adsorption isotherms of both NIP-NMRP and NIP-FRP were similar, whereas there is a large difference between those of MIP-NMRP and MIP-FRP. Modeling allows a more detailed discussion of the influence of the polymerization process. In particular, it teaches whether enhanced adsorption comes from higher affinity or larger density of molecular imprints.

The adsorption to MIP-NMRP was much higher than to MIP-FRP, as it has already been disclosed in section 2.4 (Figure 7). As a supplementary outcome of modeling, the larger adsorption to MIPs (with respect to NIPs) is not due to a higher affinity of DCHA to molecular imprints but to the formation of supplementary adsorption sites during the templated polymerization (Table 2). Indeed, the binding constants of the MIP and NIP are of the same order of magnitude; the adsorption capacity Q_{\max} of the MIP-NMRP, which is the sum of $Q_{\max,s}$ and $Q_{\max,ns}$, is twice higher than for the NIP-NMRP. A smaller ratio of 1.5 was observed for the FRP process. The density of molecular imprints $Q_{\max,s}$ is twice higher for the MIP-NMRP than for the MIP-FRP. This is not due to a higher specific surface area of the MIP-NMRP because there is only a slight difference of BET area ($17 \text{ m}^2\cdot\text{g}^{-1}$ for the MIP-NMRP against $14 \text{ m}^2\cdot\text{g}^{-1}$ for the MIP-FRP). The ratio of the Q_{\max} of MIP and NIP can be considered as an imprinting factor (IF as in eq. 3) that accounts for the adsorption behavior over the whole concentration range better than at a single concentration. The higher adsorption to MIP-NMRP compared to MIP-FRP is also not due to the higher affinity to molecular imprints, but to a larger density of molecular imprints. This conclusion is at variance with statements claiming that higher adsorption to MIP prepared by controlled radical polymerization is due to better homogeneity of cross-links that causes a higher affinity to molecular imprints [6]. The present result partly agree with those of Zu *et al.* using ATRP [16,17] and Ma *et al.* using RAFT [18] showing that the same affinity for the molecular imprints in materials prepared by RDRP and FRP. However, these latter authors also reported that the surface density of molecular imprints was the same for RDRP and FRP, whereas we presently disclose a higher surface density of the NMRP than the FRP.

The thermodynamic parameters of the selective and non-selective binding of DCHA to MIP-NMRP have been determined through adsorption isotherms measured at different temperatures (Figure 10A). Thermodynamic parameters such as standard Gibbs free energy $\Delta_{\text{ads}}G^0$, standard enthalpy $\Delta_{\text{ads}}H^0$ and standard entropy $\Delta_{\text{ads}}S^0$ of adsorption were estimated from the temperature dependence of equilibrium binding constants K for each site using the van't Hoff equation:

$$\ln(K) = \frac{\Delta_{\text{ads}}S^0}{R} - \frac{\Delta_{\text{ads}}H^0}{RT} \quad (\text{eq. 7})$$

where R ($8.314 \text{ J}\cdot\text{mol}^{-1}\cdot\text{K}^{-1}$) is the gas constant, T is the absolute temperature, and K is the binding constant for either selective or non-selective adsorption. From the slope and intercept of the plots of $\log(K)$ vs $1/T$, the values of the standard enthalpy ($\Delta_{\text{ads}}H^0$) and standard entropy ($\Delta_{\text{ads}}S^0$) were calculated.

The variations of $\log(K)$ against $1/T$ were linear (Figure 10B), showing that the values of $\Delta_{\text{ads}}H^0$ and $\Delta_{\text{ads}}S^0$ did not significantly vary in the temperature range studied. Thus, $\Delta_{\text{ads}}H^0 = -0.6 \text{ kJ}\cdot\text{mol}^{-1}$ and $\Delta_{\text{ads}}S^0 = 82.4 \text{ J}\cdot\text{mol}^{-1}\cdot\text{K}^{-1}$ for the selective adsorption onto molecular imprints; and $\Delta_{\text{ads}}H^0 = -45.0 \text{ kJ}\cdot\text{mol}^{-1}$ and $\Delta_{\text{ads}}S^0 = -68.9 \text{ J}\cdot\text{mol}^{-1}\cdot\text{K}^{-1}$ for the non-selective adsorption off the molecular imprints.

The standard enthalpy of non-selective adsorption off molecular imprints was strongly negative. Such exothermic adsorption process suggests the formation of strong hydrogen bonds between DCHA and carboxylic acids. Upon adsorption, DCHA forms hydrogen bonds with the carboxylic acid groups, while hydrogen bonds between water and both DCHA and carboxylic acids are broken at the same time. $\Delta_{\text{ads}}H^0$ is the balance of all these processes. The enthalpic contribution to the standard Gibbs free energy is higher than the entropic one ($-T\Delta_{\text{ads}}S^0$), so that $\Delta_{\text{ads}}G^0$ assumes a negative value.

The selective adsorption onto molecular imprints was athermal. It is expected that strong hydrogen bonds between DCHA and carboxylic acid groups still operate in the adsorption process to molecular imprints. The athermal process results from a compensation of exo- and endothermic processes, namely formation of hydrogen bonds between DCHA and carboxylic acid groups and release of water molecules hydrogen-bonded to DCHA and carboxylic acid groups. The net balance is an entropic adsorption process.

The thermodynamic parameters show that, although the affinity constants K_s and K_{ns} are almost the same, the adsorption processes to and off the molecular imprints are very different. This confirms the presence of molecular imprints with functional groups that are at different position and orientation than those apart from molecular imprints.

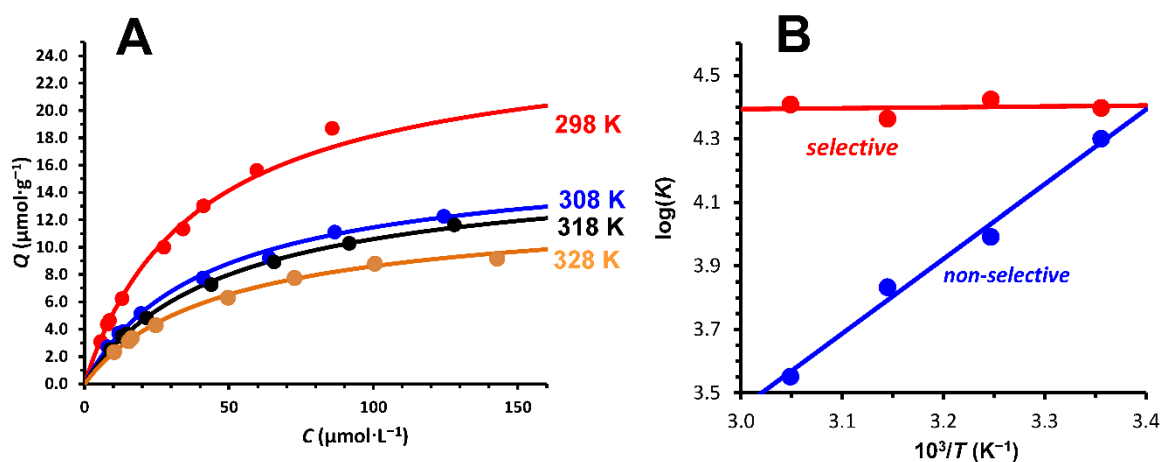


Figure 10. (A): Adsorption isotherms of DCHA onto MIP-NMRP at different temperatures (from 298 K to 328 K). (B): van't Hoff plots of $\log(K)$ against $10^3/T$ for the selective and non-selective adsorption.

2.7. Selectivity

The study of selectivity of adsorption to MIPs aims at identifying molecular recognition efficiency of materials for the target when it is in competition with other molecules in a sample. The adsorption of the target molecule is compared to the adsorption of interfering molecules under the same conditions. Two competitive interfering agents, 2,4-dichlorophenol (DCP) and 2,4,6-trichlorophenol (TCP), were chosen because these photodegradation products of OMC in chlorinated water may be found as competitive aromatic pollutants in real aqueous samples. The chemical structure of these molecules is also similar to DCHA (Figure 11). The adsorbed amounts of DCHA, DCP and TCP on MIP-NMRP or NIP-NMRP sorbents were separately measured for a single concentration of each solution using UV-vis spectroscopy in the same way as for DCHA. The distribution coefficient (K_D) corresponding to the partition of substrate between the MIP-NMRP and the solution was defined as [33,46]:

$$K_D = \frac{Q}{C} \quad (\text{eq. 8})$$

where Q ($\text{mol}\cdot\text{g}^{-1}$) is the adsorption capacity at equilibrium and C ($\text{mol}\cdot\text{L}^{-1}$) is the equilibrium concentration of molecules. The ratio of the distribution coefficients gives a selectivity coefficient α for the pair of molecules under consideration [47]:

$$\alpha = \frac{K_D(\text{DCHA})}{K_D(\text{interferent})} \quad (\text{eq. 9})$$

As shown in Figure 11 and Table 4, the adsorption capacity of the MIP-NMRP towards DCHA is much greater than that towards its interfering analogues DCP and TCP. Furthermore, the NIP-NMRP is not selective for the DCHA molecule.

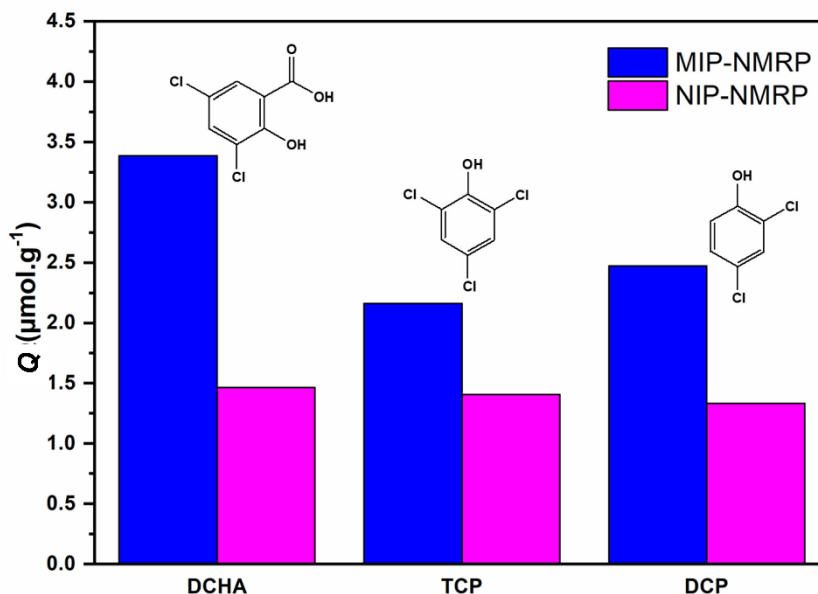


Figure 11. Adsorption capacities of MIP-NMRP and NIP-NMRP for DCHA, DCP and TCP.

The selectivity coefficients α (Table 4) provide quantitative accounts of the selectivity. Their values close to 1 for the NIP-NMRP material show that the presence of molecular imprints is definitely needed for a selective recognition of DCHA. This confirms the absence of specific sites for DCHA within the NIP-NMRP. The effect of molecular imprints can be isolated from the raw data by subtracting the adsorbed amount of the NIP to that of the MIP. This gives new corrected distribution coefficients $K_{D,corr}$ as defined in eq. 10, and a corrected selectivity coefficient α_{corr} was calculated as defined in eq. 9

$$K_{D,corr} = \frac{Q(MIP) - Q(NIP)}{C} \quad (\text{eq. 10})$$

Such a correction for the non-selective adsorption to MIP highlights the effect of molecular imprints as given in Table 4.

Table 4. Adsorption of DCHA and competitive interfering compounds onto MIP-NMRP and NIP-NMRP sorbents.

Compounds	NIP-NMRP		MIP-NMRP			
	K_D	α	K_D	α	$K_{D,corr}$	α_{corr}
DCHA	0.094	–	0.86	–	0.77	–
DCP	0.088	1.07	0.26	3.3	0.17	4.5
TCP	0.083	1.13	0.175	4.9	0.092	8.3

All these results clearly reveal that the MIP material exhibits good affinity and excellent selectivity for DCHA molecules, which is suitable for the application of this material for purification and pre-concentration techniques such as solid-phase extraction (SPE).

3. Conclusion

The adsorption properties of molecularly imprinted polymers prepared by means of nitroxide mediated radical polymerization have been compared using those of a material prepared by free radical polymerization. Nitroxide-mediated copolymerization of methacrylic acid and 10% styrene together with the EGDMA cross-linking agent and silica nanoparticles grafted with methacrylic monomer yielded small particles of a composite MIP material loaded with silica. The simple comparison of adsorbed amounts of the DCHA template molecule showed that both NMRP and FRP MIPs were actually imprinted by DCHA and that the MIP-NMRP material could bind more DCHA than the MIP-FRP. Similar results have already been reported in several instances in the literature. Modeling the adsorption isotherm allowed separating the contributions of affinity of molecular imprints for DCHA and density of molecular imprints. It has been demonstrated that the enhanced adsorption to the MIP-NMRP was caused by a higher density of molecular imprints than the MIP-FRP, the affinity for DCHA being the same for both MIP-NMRP and MIP-FRP. The same hydrogen bonding interactions of the carboxylic acid groups of poly(methacrylic acid) and the phenol group of DCHA operate in all MIP and NIP materials. The excellent selectivity and affinity for DCHA characterized by a high IF of 2 in a low concentration range, the good selectivity of DCHA adsorption against its structural analogues DCP and TCP and the quite fast kinetics of adsorption make the MIP-NMRP a sorbent material able to extract a high capacity of DCHA from aqueous media in the framework of an application to SPE.

Acknowledgments

This work was supported by the “PHC Utique” program for French-Tunisian cooperation (project number 19G1204). We are grateful to Laurent Vanoye and Yann Mourer (laboratory of Catalysis, Polymerisation, Process and Materials (CP2M), University of Lyon 1) for the BET measurements.

References

-
- [1] B. Sellergren (ed.). *Molecularly Imprinted Polymers. Man-made Mimics of Antibodies and their Applications in Analytical Chemistry*. Elsevier, Amsterdam (2001).

-
- [2] K. Karim, F. Breton, R. Rouillon, E.V. Piletska, A. Guerreiro, I. Chianella, S.A. Piletsky, How to find effective functional monomers for effective molecularly imprinted polymers? *Adv. Drug Deliv. Rev.* 57 (2005) 1795–1808. doi: [10.1016/j.addr.2005.07.013](https://doi.org/10.1016/j.addr.2005.07.013)
- [3] I.A. Nicholls, S. Chavan, K. Golker, B.C.G. Karlsson, G.D. Olsson, A.M. Rosengren, S. Suriyanarayanan, J.G. Wiklander, Theoretical and computational strategies for the study of the molecular imprinting process and polymer performance. In: *Molecularly Imprinted Polymers in Biotechnology*, B. Mattiasson, L. Ye (eds.), *Adv. Biochem. Eng. Biotechnol.* 150 (2015) 25–50. doi: [10.1007/10_2015_318](https://doi.org/10.1007/10_2015_318)
- [4] S. Beyazit, B. Tse Sum Bui, K. Haupt, C. Gonzato, Molecularly imprinted polymer nanomaterials and nanocomposites by controlled/living radical polymerization, *Prog. Polym. Sci.* 62 (2016) 1–21. doi: [10.1016/j.progpolymsci.2016.04.001](https://doi.org/10.1016/j.progpolymsci.2016.04.001)
- [5] H. Zhang, Recent advances in macromolecularly imprinted polymers by controlled radical polymerization techniques, *Mol. Impr.* 3 (2015) 35–46. doi: [10.1515/molim-2015-0005](https://doi.org/10.1515/molim-2015-0005)
- [6] M. Bompert, K. Haupt, Molecularly imprinted polymers and controlled/living radical polymerization, *Aust. J. Chem.* 62 (2009) 751–761. doi: [10.1071/CH09124](https://doi.org/10.1071/CH09124)
- [7] V.D. Salian, M.E. Byrne, Living radical polymerization and molecular imprinting: Improving polymer morphology in imprinted polymers, *Macromol. Mater. Eng.* 298 (2013) 379–390. doi: [10.1002/mame.201200191](https://doi.org/10.1002/mame.201200191)
- [8] N. Ide, T. Fukuda, Nitroxide-controlled free-radical copolymerization of vinyl and divinyl monomers. Evaluation of pendant-vinyl reactivity, *Macromolecules* 30 (1997) 4268–4271. doi: [10.1021/ma9700946](https://doi.org/10.1021/ma9700946)
- [9] A.R. Wang, S. Zhu, Branching and gelation in atom transfer radical polymerization of methyl methacrylate and ethylene glycol dimethacrylate, *Polym. Eng. Sci.* 45 (2005) 720–727. doi: [10.1002/pen.20326](https://doi.org/10.1002/pen.20326)
- [10] Q. Yu, S. Xu, H. Zhang, Y. Ding, S. Zhu, Comparison of reaction kinetics and gelation behaviors in atom transfer, reversible addition–fragmentation chain transfer and conventional free radical copolymerization of oligo(ethylene glycol) methyl ether methacrylate and oligo(ethylene glycol) dimethacrylate, *Polymer* 50 (2009) 3488–3494. doi: [10.1016/j.polymer.2009.05.032](https://doi.org/10.1016/j.polymer.2009.05.032)
- [11] K. Kanamori, J. Hasegawa, K. Nakanishi, T. Hanada, Facile synthesis of macroporous cross-linked methacrylate gels by atom transfer radical polymerization, *Macromolecules* 41 (2008) 7186–7193. doi: [10.1021/ma800563p](https://doi.org/10.1021/ma800563p)
- [12] E. Beyou, E. Bourgeat-Lami, Organic–inorganic hybrid functional materials by nitroxide-mediated polymerization, *Prog. Polym. Sci.* 121 (2021) 101434. doi: [10.1016/j.progpolymsci.2021.101434](https://doi.org/10.1016/j.progpolymsci.2021.101434)
- [13] A. Anene, R. Kalfat, Y. Chevalier, S. Hbaieb, Molecularly imprinted polymer-based materials as thin films on silica supports for efficient adsorption of Patulin, *Colloids Surfaces A: Physicochem. Eng. Aspects* 2016, 497, 293–303. doi: [10.1016/j.colsurfa.2016.03.005](https://doi.org/10.1016/j.colsurfa.2016.03.005)
- [14] S. Boonpangrak, M.J. Whitcombe, V. Prachayasittikul, K. Mosbach, L. Yea, Preparation of molecularly imprinted polymers using nitroxide-mediated living radical polymerization, *Biosensors Bioelectronics* 22 (2006) 349–354. doi: [10.1016/j.bios.2006.04.014](https://doi.org/10.1016/j.bios.2006.04.014)
- [15] A.D. Vaughan, J.B. Zhang, M.E. Byrne, Enhancing therapeutic loading and delaying transport via molecular imprinting and living/controlled polymerization, *AIChE J.* 56 (2010) 268–279. doi: [10.1002/aic.11949](https://doi.org/10.1002/aic.11949)

-
- [16] B. Zu, G. Pan, X. Guo, Y. Zhang, H. Zhang, Preparation of molecularly imprinted polymer microspheres via atom transfer radical precipitation polymerization, *J. Polym. Sci.: Part A: Polym. Chem.* 47 (2009) 3257–3270. doi: [10.1002/pola.23389](https://doi.org/10.1002/pola.23389)
- [17] B. Zu, Y. Zhang, X. Guo, H. Zhang, Preparation of molecularly imprinted polymers via atom transfer radical “bulk” polymerization, *J. Polym. Sci.: Part A: Polym. Chem.* 48 (2010) 532–541. doi: [10.1002/pola.23750](https://doi.org/10.1002/pola.23750)
- [18] Y. Ma, G. Pan, Y. Zhang, X. Guo, H. Zhang, Comparative study of the molecularly imprinted polymers prepared by reversible addition–fragmentation chain transfer “bulk” polymerization and traditional radical “bulk” polymerization, *J. Mol. Recognit.* 26 (2013) 240–251. doi: [10.1002/jmr.2267](https://doi.org/10.1002/jmr.2267)
- [19] B. Charleux, J. Nicolas, O. Guerret, Theoretical expression of the average activation-deactivation equilibrium constant in controlled/living free-radical copolymerization operating via reversible termination. Application to a strongly improved control in nitroxide-mediated polymerization of methyl methacrylate, *Macromolecules* 38 (2005) 5485–5492. doi: [10.1021/ma050087e](https://doi.org/10.1021/ma050087e)
- [20] J. Nicolas, C. Dire, L. Mueller, J. Belleney, B. Charleux, S.R.A. Marque, D. Bertin, S. Magnet, L. Couvreur, Living character of polymer chains prepared via nitroxide-mediated controlled free-radical polymerization of methyl methacrylate in the presence of a small amount of styrene at low temperature, *Macromolecules* 39 (2006) 8274–8282. doi: [10.1021/ma061380x](https://doi.org/10.1021/ma061380x)
- [21] J. Nicolas, L. Mueller, C. Dire, K. Matyjaszewski, B. Charleux, Comprehensive modeling study of nitroxide-mediated controlled/living radical copolymerization of methyl methacrylate with a small amount of styrene, *Macromolecules* 42 (2009) 4470–4478. doi: [10.1021/ma900515v](https://doi.org/10.1021/ma900515v)
- [22] C. Dire, B. Charleux, S. Magnet, L. Couvreur, Nitroxide-mediated copolymerization of methacrylic acid and styrene to form amphiphilic diblock copolymers, *Macromolecules* 40 (2007) 1897–1903. doi: [10.1021/ma062750k](https://doi.org/10.1021/ma062750k)
- [23] X.G. Qiao, P.-Y. Dugas, B. Charleux, M. Lansalot, E. Bourgeat-Lami, Nitroxide-mediated polymerization-induced self-assembly of amphiphilic block copolymers with a pH/temperature dual sensitive stabilizer block, *Polym. Chem.* 8 (2017) 4014–4029. doi: [10.1039/c7py00595d](https://doi.org/10.1039/c7py00595d)
- [24] R. Zhou, G. Lu, Z. Yan, X. Bao, P. Zhang, R. Jiang, Bioaccumulation and biochemical effects of ethylhexyl methoxy cinnamate and its main transformation products in zebrafish, *Aquatic Toxicol.* 214 (2019) 105241. doi: [10.1016/j.aquatox.2019.105241](https://doi.org/10.1016/j.aquatox.2019.105241)
- [25] H. Sharifan, Alarming the impacts of the organic and inorganic UV blockers on endangered coral’s species in the Persian Gulf: A scientific concern for coral protection *Sustainable Futures* 2 (2020) 100017. doi: [10.1016/j.sftr.2020.100017](https://doi.org/10.1016/j.sftr.2020.100017)
- [26] B. Nataraj, K. Maharajan, D. Hemalatha, B. Rangasamy, N. Arul, M. Ramesh, Comparative toxicity of UV-filter Octyl methoxycinnamate and its photoproducts on zebrafish development, *Sci. Total Environ.* 718 (2019) 134546. doi: [10.1016/j.scitotenv.2019.134546](https://doi.org/10.1016/j.scitotenv.2019.134546)
- [27] M. Lorigo, M. Mariana, E. Cairrao, Photoprotection of ultraviolet-B filters: Updated review of endocrine disrupting properties, *Steroids* 131 (2018) 46–58. doi: [10.1016/j.steroids.2018.01.006](https://doi.org/10.1016/j.steroids.2018.01.006)
- [28] A.G. Mayes, K. Mosbach, Molecularly imprinted polymers: useful materials for analytical chemistry? *Trends Anal. Chem.* 16 (1997) 321–332. doi: [10.1016/S0165-9936\(97\)00037-X](https://doi.org/10.1016/S0165-9936(97)00037-X)
- [29] J.L. Couturier, O. Guerret, *PCT Int. Appl.* WO0212149 (2002).

-
- [30] W. Thiessen, T. Wolff, New and improved routes to alkoxyamine initiators for controlled radical polymerisation, *Designed Monomers Polym.* 8 (2005) 397–407. doi: [10.1163/1568555054937926](https://doi.org/10.1163/1568555054937926)
- [31] N. Amaly, G. Istamboulie, A.Y. El-Moghazy, T. Noguer, Reusable molecularly imprinted polymeric nanospheres for diclofenac removal from water samples, *J. Chem. Res.* 45 (2021) 102–110. doi: [10.1177/1747519820925998](https://doi.org/10.1177/1747519820925998)
- [32] N. Delgado, A. Capparelli, A. Navarro, D. Marino, Pharmaceutical emerging pollutants removal from water using powdered activated carbon: Study of kinetics and adsorption equilibrium, *J. Environ. Management* 236 (2019) 301–308. doi: [10.1016/j.jenvman.2019.01.116](https://doi.org/10.1016/j.jenvman.2019.01.116)
- [33] R.J. Ansell, Characterization of the binding properties of molecularly imprinted polymers. In: *Molecularly Imprinted Polymers in Biotechnology*, B. Mattiasson, L. Ye (eds.), *Adv. Biochem. Eng. Biotechnol.* 2015, 150, 51–93. doi: [10.1007/10_2015_316](https://doi.org/10.1007/10_2015_316)
- [34] F. Sbardella, M.P. Bracciale, M.L. Santarelli, J.M. Asua, Waterborne modified-silica/acrylates hybrid nanocomposites as surface protective coatings for stone monuments, *Prog. Org. Coatings* 149 (2020) 105897. doi: [10.1016/j.porgcoat.2020.105897](https://doi.org/10.1016/j.porgcoat.2020.105897)
- [35] F. Pardal, V. Lapinte, J.-J. Robin, Modification of silica nanoparticles by grafting of copolymers containing organosilane and fluorine moieties, *J. Polym. Sci. Part A: Polym. Chem.* 47 (2009) 4617–4628. doi: [10.1002/pola.23513](https://doi.org/10.1002/pola.23513)
- [36] C. Ayadi, A. Anene, R. Kalfat, Y. Chevalier, S. Hbaieb, Molecular imprints frozen by strong intermolecular interactions in place of cross-linking, *Chem. Eur. J.* 27 (2021) 2175–2183. doi: [10.1002/chem.202004580](https://doi.org/10.1002/chem.202004580)
- [37] F.A. Trikka, K. Yoshimatsu, L. Ye, D.A. Kyriakidis, Molecularly imprinted polymers for histamine recognition in aqueous environment, *Amino Acids* 43 (2012) 2113–2124. doi: [10.1007/s00726-012-1297-8](https://doi.org/10.1007/s00726-012-1297-8)
- [38] A. Konishi, S. Takegami, S. Akatani, R. Takemoto, T. Kitade, Potentiometric and ¹H NMR spectroscopic studies of functional monomer influence on histamine-imprinted polymer-modified potentiometric sensor performance, *J. Anal. Bioanal. Tech.* 8 (2017) 1000378. doi: [10.4172/2155-9872.1000378](https://doi.org/10.4172/2155-9872.1000378)
- [39] L.A. Tom, N.A. Schneck, C. Walter, Improving the imprinting effect by optimizing template:monomer:cross-linker ratios in a molecularly imprinted polymer for sulfadimethoxine, *J. Chromatogr. B* 909 (2012) 61–64. doi: [10.1016/j.jchromb.2012.10.020](https://doi.org/10.1016/j.jchromb.2012.10.020)
- [40] C. Ayadi, A. Anene, R. Kalfat, Y. Chevalier, S. Hbaieb, Molecularly imprinted polyaniline on silica support for the selective adsorption of benzophenone-4 from aqueous media, *Colloids Surfaces A: Physicochem. Eng. Aspects* 567 (2019) 32–42. doi: [10.1016/j.colsurfa.2019.01.042](https://doi.org/10.1016/j.colsurfa.2019.01.042)
- [41] R.I. Moustafine, I.M. Zaharov, V.A. Kemenova, Physicochemical characterization and drug release properties of Eudragit® E PO/Eudragit® L 100-55 interpolyelectrolyte complexes, *Eur. J. Pharm. Biopharm.* 2006, 63, 26–36. doi: [10.1016/j.ejpb.2005.10.005](https://doi.org/10.1016/j.ejpb.2005.10.005)
- [42] C. Gonzato, P. Pasetto, F. Bedoui, P.-E. Mazeran, K. Haupt, On the effect of using RAFT and FRP for the bulk synthesis of acrylic and methacrylic molecularly imprinted polymers, *Polym. Chem.* 5 (2014) 1313–1322. doi: [10.1039/c3py01246h](https://doi.org/10.1039/c3py01246h)
- [43] A.G. Mayes, *Molecularly Imprinted Polymers. Man-made Mimics of Antibodies and their Applications in Analytical Chemistry*, ed. B. Sellergren, Elsevier, Amsterdam (2001), Chap. 12, pp. 305–324.
- [44] I. Langmuir, The adsorption of gases on plane surfaces of glass, mica and platinum, *J. Am. Chem. Soc.* 40 (1918) 1361–1403. doi: [10.1021/ja02242a004](https://doi.org/10.1021/ja02242a004)

-
- [45] M. Volmer, Thermodynamische Folgerungen ans der Zustandsgleichnung für adsorbierte Stoffe, *Z. Phys. Chem.* 115 (1925) 253–260. doi: [10.1515/zpch-1925-11519](https://doi.org/10.1515/zpch-1925-11519)
- [46] F. An, B. Gao, X. Feng, Adsorption and recognizing ability of molecular imprinted polymer MIP-PEI/SiO₂ towards phenol, *J. Hazard. Mater.* 157 (2008) 286–292. doi: [10.1016/j.jhazmat.2007.12.095](https://doi.org/10.1016/j.jhazmat.2007.12.095)
- [47] E. Decompte, V. Lobaz, M. Monperrus, E. Deniau, M. Save, Molecularly imprinted polymer colloids synthesized by miniemulsion polymerization for recognition and separation of nonylphenol, *ACS Appl. Polym. Mater.* 2 (2020) 3543–3556. doi: [10.1021/acsapm.0c00560](https://doi.org/10.1021/acsapm.0c00560)

SUPPORTING INFORMATION

The enhanced adsorption properties of molecular imprinted polymer material prepared using nitroxide-mediated Radical Deactivation Reversible Polymerization

Soumaya Kouki^{a,b,c,d}, Najeh Jaoued-Grayaa^d, Amira Anene^d, Emmanuel Beyou, Yves Chevalier^{b*}, Souhaira Hbaieb^{a*}

a) Laboratoire de Recherche: Caractérisations, Applications et Modélisation de Matériaux, Université de Tunis El Manar, Faculté des Sciences de Tunis, Campus universitaire El Manar, Tunisia.

b) Laboratoire d'Automatique, de Génie des Procédés et de Génie Pharmaceutique, Université de Lyon 1, UMR 5007 CNRS, 69622 Villeurbanne Cedex, France.

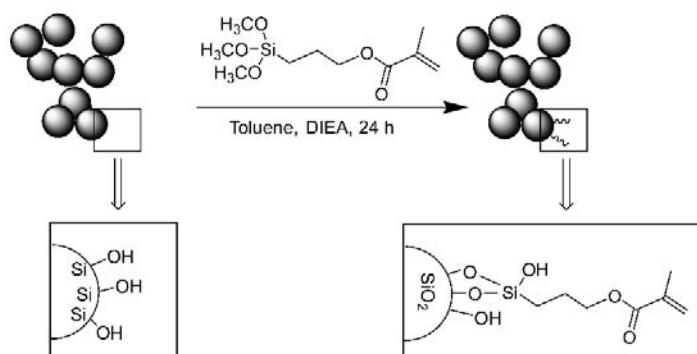
c) Laboratoire Ingénierie des Matériaux Polymères, Université de Lyon 1, UMR 5223, 69622 Villeurbanne, France.

d) Unité Spécialisée de développement des techniques analytiques, Institut National de Recherche et d'Analyse Physico-chimique, Biotechpole Sidi-Thabet, 2020 Ariana, Tunisia.

S11. Grafting of MPTS onto silica nanoparticles

The two grafting processes used in our work are:

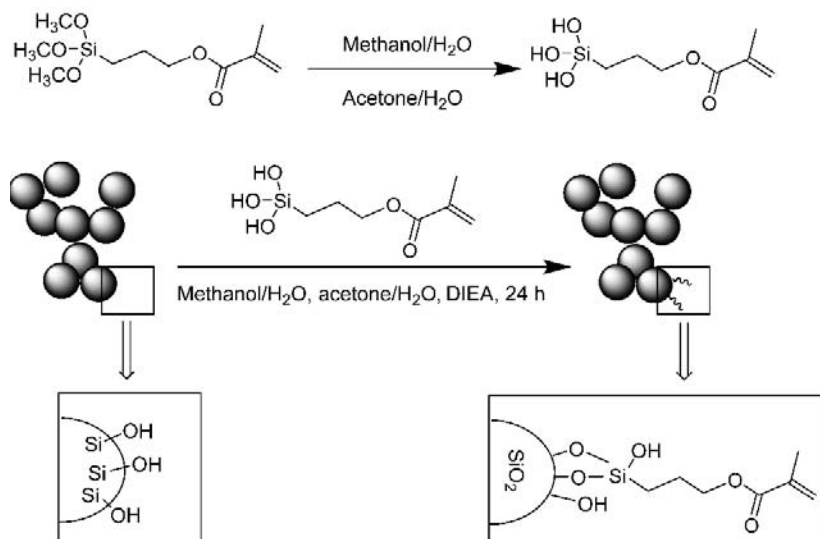
- Anhydrous toluene was employed to afford a monolayer of methacryloyl groups at the SiO₂ surface. The silanols of the silica surface and the methoxy groups of MPTS undergo a direct reaction using DIEA as catalyst causing the deprotonation of silica OH groups according to the following reaction ([Scheme S1](#)):



Scheme S1. Grafting reaction yielding a monolayer of methacryloyl silane.

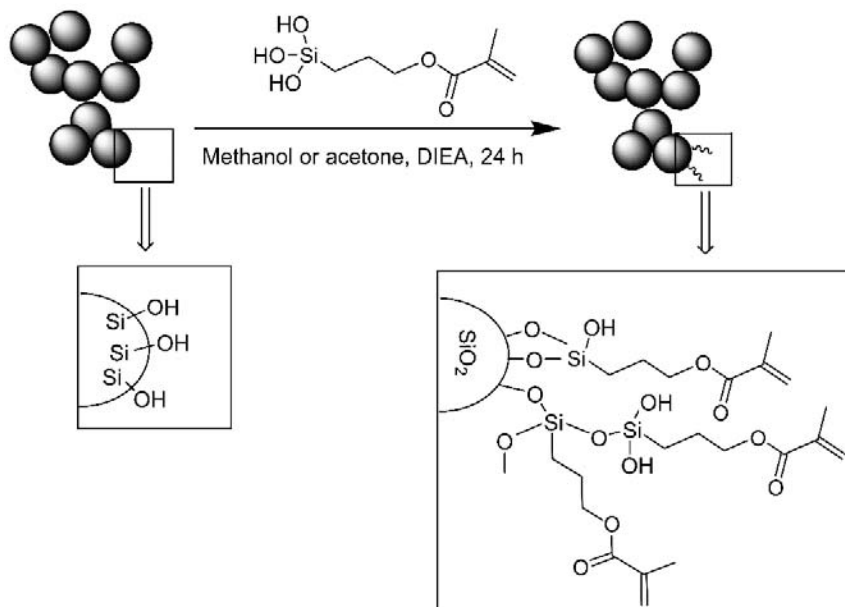
- The methanol/water or acetone/water solvents were used in the wet process. Silanols were generated via the hydrolysis reaction of methoxy groups of MPTS. They bound by hydrogen

interactions with the surface hydroxyl groups of silica and their condensation on the surface subsequently occurred together with the release of a water molecule (Scheme S2).



Scheme S2. Hydrolysis of methoxysilyl groups of MPTS and its condensation to silica surface.

A side-reaction is also possible in this latter case; the silanol groups of hydrolyzed MPTS may undergo a polycondensation reaction leading to the formation of a thick layer of polysiloxane strands bound to the surface of silica according to Scheme S3 [1].



Scheme S3. Possible surface polycondensation side-reaction.

Grafting of MPTS onto silica was performed using three different solvents: anhydrous toluene, acetone/water, and methanol/water (Table S1).

The grafting densities (Table S1) were determined by thermogravimetric analysis (TGA). The mass loss was determined between 200 °C and 600 °C. The grafting densities (d) of MPTS onto silica were calculated from Eq. S1 [2–4]:

$$d \text{ (}\mu\text{mol} \cdot \text{m}^{-2}\text{)} = \frac{\frac{m(\text{SiO}_2\text{-MPTS})}{100 - m(\text{SiO}_2\text{-MPTS})} \frac{m(\text{SiO}_2)}{100}}{M \times A_{\text{sp}}} \times 10^6 \quad (\text{Eq. S1})$$

where $m(\text{SiO}_2\text{-MPTS})$ is the % mass loss in the temperature range (200–600 °C), $m(\text{SiO}_2)$ is the % mass loss of pristine fumed silica in the same temperature range, $M = 127 \text{ g} \cdot \text{mol}^{-1}$ is the molar mass of the propylmethacrylate moiety lost by thermal degradation, and $A_{\text{sp}} = 200 \text{ m}^2 \cdot \text{g}^{-1}$ is the specific surface area of fumed silica.

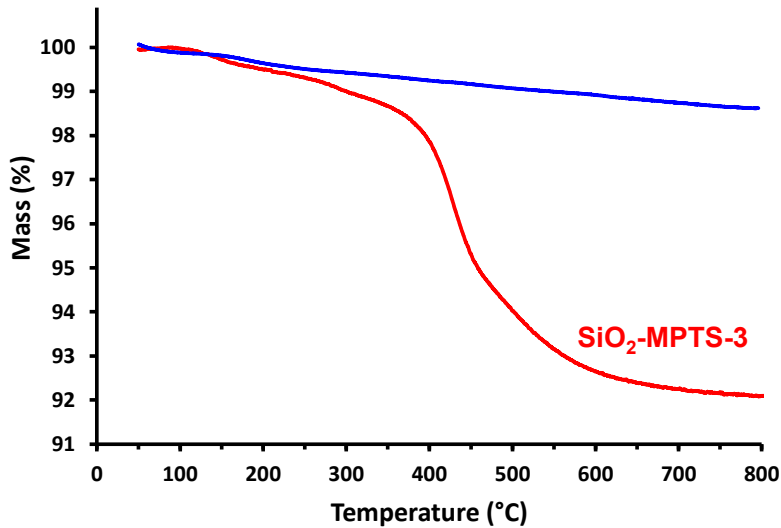


Figure S1. TGA curves of SiO₂-MPTS-3 and bare SiO₂.

The grafting densities of modified silica were also determined from the contents of carbon (%C) using Eq. S2 where 12 is the molar mass of carbon and 7 is the number of carbon atoms in the grafted propylmethacrylate moiety:

$$d \text{ (}\mu\text{mol} \cdot \text{m}^{-2}\text{)} = \frac{1}{A_{\text{sp}}} \frac{1}{\frac{100 \times 12 \times 7}{\%C} - 1} \times 10^6 \quad (\text{Eq. S2})$$

Both determinations of the grafted density were in good agreement with each other. The determination by elemental analysis of carbon is though more accurate because the calculation of grafting density from TGA curves requires considering a rather subjective choice of temperature range.

Table S1. Grafting densities of SiO₂-MPTS determined by TGA and elemental analyses.

Grafted silica	Solvent	Silane concentration (g L ⁻¹)	Elemental analysis of carbon (%)	Calculated surface density (μmol m ⁻²)	
				from elemental analysis	from TGA
SiO ₂ -MPTS-1	Anhydrous toluene	12.5	3.34	2.0	2.0
SiO ₂ -MPTS-2	Anhydrous toluene	17.5	3.70	2.2	2.0
SiO ₂ -MPTS-3	Anhydrous toluene	25.0	3.85	2.3	2.8
SiO ₂ -MPTS-4	MeOH/H ₂ O (95/5 v/v)	25.0	4.17	2.5	2.8
SiO ₂ -MPTS-5	Acetone/H ₂ O (95/5 v/v)	25.0	4.44	2.7	3.2

The FTIR spectrum of grafted silica (Figure S2) showed a strong band of Si–O–Si stretching vibration at 1200 cm⁻¹ and additional characteristic bands arising from organic moieties of MPTS at 1715 cm⁻¹ and 1632 cm⁻¹. The latter respectively corresponded to the carbonyl (C=O) and double bond (C=C) of the methacrylate groups immobilized onto the silica surface.

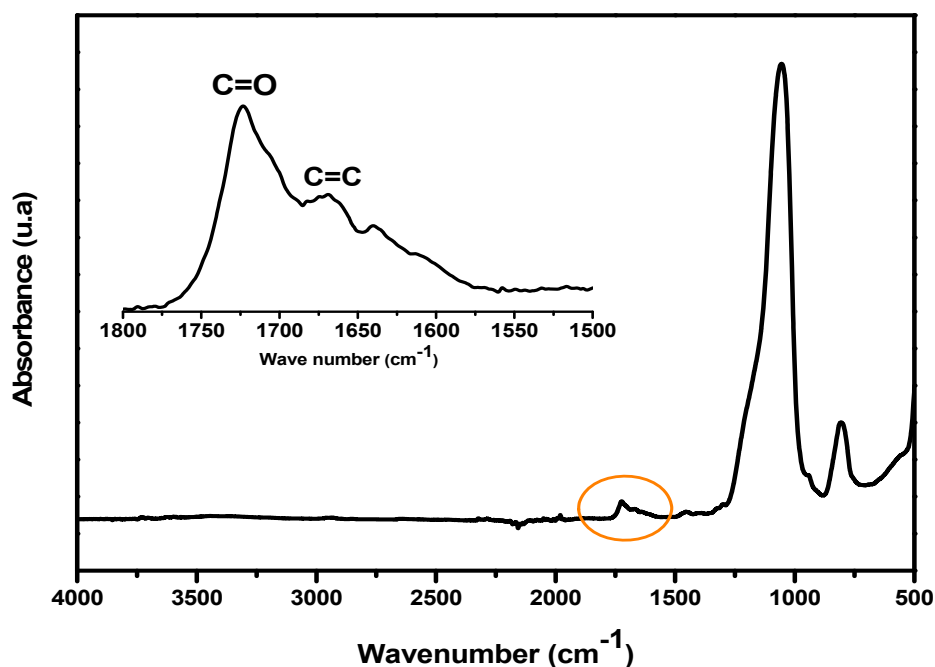


Figure S2. FTIR spectrum of SiO₂-MPTS-3.

SI2. ¹H NMR study of pre-polymerization mixture

The nature of interaction and the highest affinity between methacrylic acid monomer and DCHA molecule were investigated using ¹H NMR. DCHA protons were observed as a singlet for HA at 2.700 ppm, a doublet for HB at 7.923 ppm (⁴J_{HB-HC} = 2.5 Hz) and a doublet for HC 7.999 ppm (⁴J_{HB-HC} = 2.5 Hz) as shown in Figure S3 and Table S2.

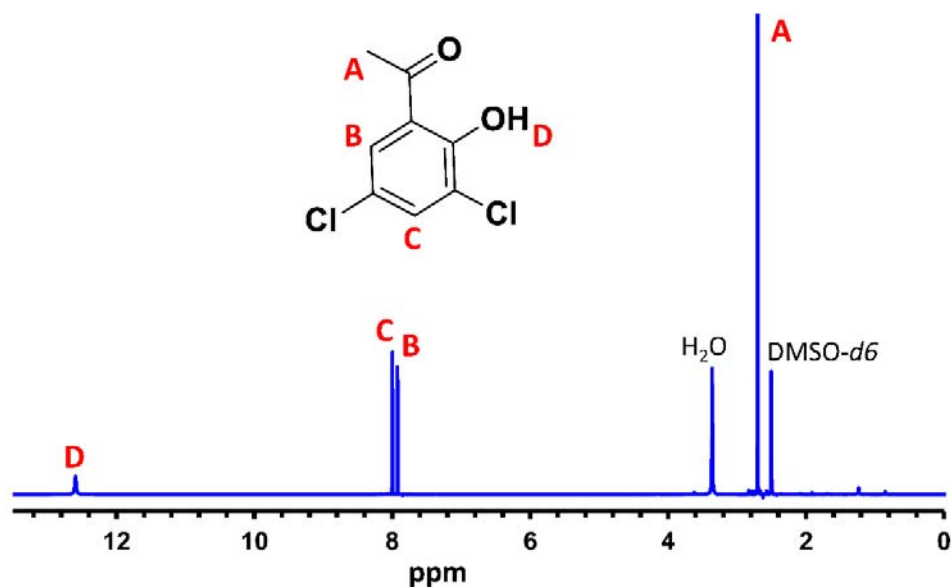


Figure S3. ¹H NMR spectrum of DCHA in DMSO-*d*₆.

Table S2. ¹H NMR chemical shifts (ppm) of HA, HB, and HC protons of DCHA, either pure or in presence of the MAA functional monomer in DMSO-*d*₆.

MAA/DCHA mole ratio	δ HA	δ HB	δ HC
0	2.7005	7.9229	7.9993
3	2.6925	7.8919	7.9834
4	2.6861	7.8888	7.9773
6	2.6838	7.8674	7.9706
8	2.6815	7.8650	7.9671

SI3. Characterization of molecularly imprinted polymers

The ¹³C NMR spectra of MIP-NMRP and NIP-NMRP in Figure S4 clearly showed the characteristic peaks of MAA-*co*-EGDMA copolymer. The peaks at 163, 47 and 30 ppm were respectively assigned to the carbonyl groups of (–CH₂–O–C=O), the methylene groups –CH–CH₂–

groups and CH₃ groups of the MAA-*co*-EGDMA copolymer. Low intensity peaks appearing between 120 and 140 ppm showed the presence of residual vinyl groups after polymerization. The spectrum of NIP-NMRP showed the same peaks as MIP-NMRP indicating a structural similarity between imprinted and non-imprinted materials. The ¹³C NMR spectra of MIP-NMRP and NIP-NMRP definitely showed the successful copolymerization of the grafted MPTS, MAA monomer and EGDMA cross-linker.

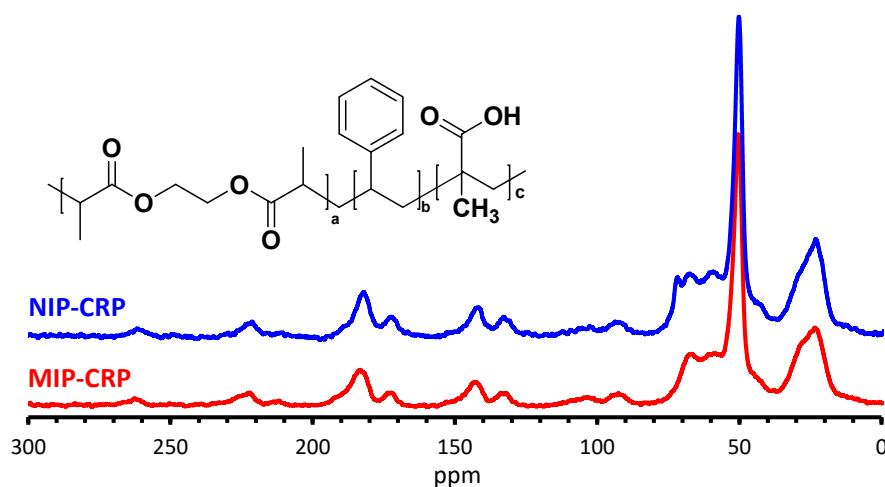


Figure S4. ¹³C MAS NMR spectra of MIP-NMRP and NIP-NMRP.

TGA analysis allowed the determination of the amount of polymer grafted to the SiO₂-MPTS material. The TGA curves of MIP-NMRP and NIP-NMRP (Figure S5) showed two mass losses starting at 140 °C and 300 °C. The first mass loss was due to the removal of adsorbed water and the second mass loss occurring at 300–600 °C was caused by the decomposition of organic components. This mass loss is the polymer content expressed as the mass of copolymer per unit mass of material ($\% = 100 \times \text{g} \cdot \text{g}^{-1}$).

The same mass fraction of polymer was calculated from elemental analyses of carbon (%C) as:

$$\chi(\text{polymer}) (\%) = 100 \frac{\%C}{\%C(\text{copolymer})} \quad (\text{Eq. S3})$$

where %C(copolymer) = 56.25 % is the carbon content of the MMA-*co*-EGDMA 50/50 copolymer taken as the average of the homopolymers poly(MMA) (55.81 %) and poly(EGDMA) (56.47 %).

As a matter of discussion of a possible morphology as a polymer coating grafted onto the silica surface, the ‘grafting density’ was also expressed as the mass of copolymer per unit surface area of silica ($\text{g} \cdot \text{m}^{-2}$). It was calculated by Eq. S4 using the mass loss of TGA [5]:

$$d \text{ (g} \cdot \text{m}^{-2}\text{)} = \frac{\frac{m(\text{MIP})}{100-m(\text{MIP})} - \frac{m(\text{SiO}_2\text{-MPTS})}{100-m(\text{SiO}_2\text{-MPTS})}}{A_{\text{sp}}} \quad (\text{Eq. S4})$$

The same grafting density was calculated from elemental analyses of carbon (%C) as:

$$d \text{ (g} \cdot \text{m}^{-2}\text{)} = \frac{1}{A_{\text{sp}}} \frac{1}{\frac{\%C(\text{copolymer})}{\%C} - 1} \quad (\text{Eq. S5})$$

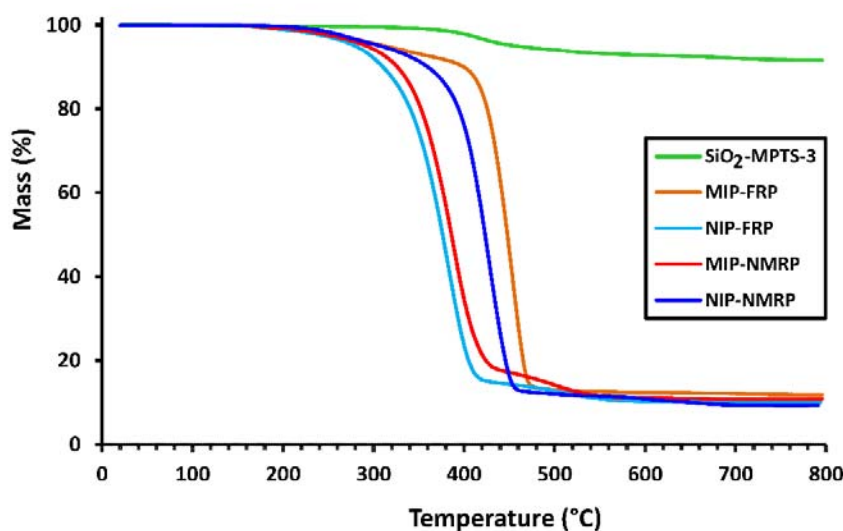


Figure S5. Thermogravimetric analyses of SiO₂-MPTS-3, NIP-NMRP, MIP-NMRP, NIP-FRP and MIP-FRP.

References

- [1] U. Goerl, A. Hunsche, A. Mueller, H.G. Koban, Investigations into the silica/silane reaction system, *Rubber Chem. Technol.* 70 (1997) 608–623. doi: [10.5254/1.3538447](https://doi.org/10.5254/1.3538447)
- [2] F. Pardal, V. Lapinte, J.-J. Robin, Modification of silica nanoparticles by grafting of copolymers containing organosilane and fluorine moieties, *J. Polym. Sci.: Part A: Polym. Chem.* 47 (2009) 4617–4628. doi: [10.1002/pola.23513](https://doi.org/10.1002/pola.23513)
- [3] P. Silakul, R. Magaraphan, Polymer electrolyte developed from natural rubber-polyacrylic acid co trimethoxysilyl propyl methacrylate grafted fumed silica and its application to dye sensitized solar cell, *Polym. Composite* 40 (2017) 304–314. doi: [10.1002/pc.24648](https://doi.org/10.1002/pc.24648)
- [4] C. Bartholome, E. Beyou, E. Bourgeat-Lami, P. Chaumont, N. Zydowicz, Nitroxide-mediated polymerizations from silica nanoparticle surfaces: “graft from” polymerization of styrene using a triethoxysilyl-terminated alkoxyamine initiator, *Macromolecules* 36 (2003) 7946–7952. doi: [10.1021/ma034491u](https://doi.org/10.1021/ma034491u)
- [5] C. Ayadi, A. Anene, R. Kalfat, Y. Chevalier, S. Hbaieb, Molecularly imprinted polyaniline on silica support for the selective adsorption of benzophenone-4 from aqueous media, *Colloids Surfaces A: Physicochem. Eng. Aspects* 567 (2019) 32–42. doi: [10.1016/j.colsurfa.2019.01.042](https://doi.org/10.1016/j.colsurfa.2019.01.042)